NACA RM L55G08

NATIONAL ADVISORY COMMITTEE FOR AERONAUTICS

RESEARCH MEMORANDUM

TRANSONIC WIND-TUNNEL INVESTIGATION OF EFFECTS OF WINDSHIELD SHAPE AND CANOPY LOCATION ON THE AERODYNAMIC CHARACTERISTICS OF CANOPY-BODY COMBINATIONS

By Elden S. Cornette and Harold L. Robinson

SUMMARY

Aerodynamic data have been obtained for a fuselage forebody alone and for canopy-body configurations consisting of four different canopies mounted on a fuselage forebody. Two of the canopies had the same shape and size rearward of the windshield but one had a "flat" and the other a "vee" windshield. The remaining two canopies were located at different body stations and were geometrically similar.

The data, obtained for a Mach number range from 0.80 to 1.13, an angle-of-attack range from 0° to 10°, and an angle-of-sideslip range from -8° to 8°, indicated that the drag of the flat-windshield model was consistently lower than that of the vee-windshield model. Of the remaining forces and moments, only the lateral force was significantly affected by windshield shape, the vee-shaped windshield causing increased lateral force. Little effect of canopy location was found for the canopy-body configurations investigated.

INTRODUCTION

Recently a wind-tunnel test program was undertaken at the Langley Laboratory of the National Advisory Committee for Aeronautics to obtain aerodynamic data in the transonic and supersonic speed ranges for a series of airplane canopy models mounted on a common fuselage forebody. The primary purpose of this program was to investigate the aerodynamic loads experienced by canopy models that simulate present designs used on high-speed aircraft and to evaluate the effects of such design variables as canopy location, size, and windshield shape.

In the present investigation, both pressure-distribution and force data were obtained in the Langley 8-foot transonic tunnel for four different canopies mounted on a fuselage forebody. Presented in this paper

are the six-component force data for the canopy-body configurations as well as the forebody alone. Two of the canopies were mounted well forward on the body and had the same shape behind the windshield but one had a "flat" and the other a "vee" windshield. The two remaining canopies had a smaller maximum cross-sectional area than the first two and both had flat windshields. The two smaller canopies were located at different longitudinal positions on the body.

The Mach number range for this investigation was from 0.80 to 1.13 while the angle of attack was varied from 0° to 10° and the angle of sideslip was varied from -8° to 8°.

SYMBOLS

a	one-half major diameter of body cross-section ellipse
b	one-half minor diameter of body cross-section ellipse, a/1.25
C_A	axial-force coefficient, $\frac{\text{Axial force}}{qS}$
C_D	drag coefficient, Drag/qS
C_l	rolling-moment coefficient, $\frac{\text{Rolling moment}}{qSL}$
C_m	pitching-moment coefficient, $\frac{\text{Pitching moment}}{qSL}$
C_n	yawing-moment coefficient, $\frac{\text{Yawing moment}}{qSL}$
C_N	normal-force coefficient, $\frac{\text{Normal force}}{qS}$
C_Y	lateral-force coefficient, $\frac{\text{Lateral force}}{qS}$
c	one-half major diameter of canopy cross-section ellipse
d	one-half minor diameter of canopy cross-section ellipse
h	distance to top of round canopy, measured from straight center line of body

L	total body length, 25 inches
M	stream Mach number
P_b	base pressure coefficient, $\frac{p_b - p}{q}$
p	stream static pressure
p_b	static pressure at model base
q	stream dynamic pressure, $\rho V^2/2$
R	Reynolds number per foot of length, $\rho V/\mu$
r	radius of cross section of round canopy
S	maximum cross-sectional area of fuselage, 15.71 sq in.
u	vertical coordinate of canopy cross section
v	horizontal coordinate of canopy cross section
V	stream velocity
x	distance measured from body nose along straight center line (positive rearward)
z	vertical distance from straight center line to drooped center line of body (positive downward)
α	angle of attack
β	angle of sideslip
μ	stream viscosity
ρ	stream density

APPARATUS AND MEASUREMENTS

Models

The dimensions of the models are presented in figure 1. The fuselage is five maximum fuselage depths in length and is of elliptic cross

[redacted]

section (b = a/1.25). (See fig. 1(a).) The fuselage center line droops from a station 3.5 maximum fuselage depths rearward of the nose point in an arc so that the maximum droop at the nose is 0.2 maximum fuselage depth. The centers of the fuselage cross-section ellipses lie along this drooped center line.

The cross sections of canopies 1 and 2 (figs. 1(b) and (c)) behind the windshield (behind the 6.25-inch station) were ellipses (d = c/2.5) perpendicular to the fuselage horizontal center line with centers located on the fuselage drooped center line. Canopy 1 had a flat windshield while canopy 2 had a vee windshield. Both of these canopies were located at the forward position on the fuselage.

Canopies 3 and 4 (figs. 1(d) and (e)) were geometrically similar and had circular cross sections behind the windshield. Both canopies had flat windshields but canopy 4 was located 3.75 inches farther downstream on the fuselage than canopy 3. Unfortunately, canopy 3 was constructed slightly inaccurately and the actual measured dimensions are presented in figure 1(d). The cross-sectional area distributions of the five models are presented in figure 1(f).

Tunnel

This investigation was conducted in the Langley 8-foot transonic tunnel, which has a dodecagonal slotted test section and is capable of continuously variable operation through the speed range up to a Mach number of 1.15. The models were mounted on the conventional sting system used in the 8-foot transonic tunnel. Detailed discussions of the design and calibration of this tunnel have been presented in references 1 and 2. The uniformity of the Mach number distribution in the model region is within ±0.006. Tunnel-wall constraint and blockage corrections have not been applied to the data because such corrections are negligible. The effects of boundary-reflected disturbances are also considered negligible at the Mach numbers for which data are presented.

Tests

The models were tested at stream Mach numbers of 0.80, 0.90, 0.95, 0.99, 1.02, 1.08, and 1.13. The maximum random error in measuring the stream Mach number is believed to be about 0.003. At each Mach number the models were tested at nominal angles of attack of 0°, 5°, and 10° and at nominal angles of sideslip of 0°, $\pm 4^\circ$, and $\pm 8^\circ$. The Reynolds number per foot of length varied during the investigation and the approximate spread is shown in figure 2 plotted against Mach number.

Force and Moment Measurements

The forces and moments were measured with respect to a body-axis system by means of an internally mounted electrical strain-gage balance system. The center of the axis system was located at the 14.813-inch body station and the longitudinal axis coincided with the straight center line of the body. (See fig. 3.) The maximum cross-sectional area of the body (15.71 square inches) and the length of the body (25 inches) were used to reduce these forces and moments to coefficient form.

The pressures at the base of the model were measured and the axial force was adjusted to the condition of free-stream static pressure at the model base. Figure 4 shows the variation of base pressure coefficient with Mach number at zero angle of attack and sideslip for the five models tested. The base pressure coefficients were estimated to be accurate to within ±0.005. A block of wood having the same cross-sectional shape as the body at the 25-inch station and 1 foot long was fastened rigidly to the sting behind the model in order to reduce the flow expansion about the model base and stabilize the base pressure. The gap between the block of wood and the model was approximately 1/16 inch.

The force and moment coefficients presented in this paper are referred to the body-axis system. In addition the forces were resolved along the wind axis to obtain the drag, which also is presented. An estimate of the maximum random error in the data reported herein is presented in the following table:

Axial-force coefficient, C_A	±0.004
Drag coefficient, C_D	±0.004
Normal-force coefficient, C_N	±0.02
Lateral-force coefficient, C_Y	±0.01
Rolling-moment coefficient, C_l	±0.002
Yawing-moment coefficient, C_n	±0.002
Pitching-moment coefficient, C_m	±0.002

Angle-of-Sideslip and Angle-of-Attack Measurements

In order to facilitate sideslip-angle measurements, the model was rotated 90° before mounting on the sting support system. The sideslip angle was then measured by an electrical strain-gage pendulum device mounted internally near the base of the support sting. Sting and model deflections occurring ahead of this point as a result of forces and moments acting on the model were determined from static tests. The corrections were applied to the sideslip angle.

[redacted]

The angle of attack was obtained by inserting 0°-, 5°-, and 10°-bent couplings in the support sting. The incremental change in angle of attack due to load was determined from static tests and applied to the zero-load angle of attack. The maximum deflection due to load was approximately 0.3°. The angles of sideslip and attack reported herein are accurate within 0.1°.

RESULTS AND DISCUSSION

Basic Data

The force and moment coefficients for the five models are presented in figures 5 to 9. The flagged symbols indicate data at positive sideslip angles and the sense of C_Y C_l, and C_n has been reversed for these data points. As mentioned previously, canopy 3 was not accurately constructed and the discrepancy in the corresponding negative and positive sideslip-angle data is apparent for the axial-force coefficient (fig. 8).

Effect of Windshield Shape

The effect of windshield shape is illustrated in figure 10, where data for canopy 1 (flat windshield), canopy 2 (vee-shaped windshield), and the body alone have been plotted against Mach number. It can be seen that the shape of the windshield did not have an important effect on the normal-force coefficient (fig. 10(a)). At a sideslip angle of -8°, a reduction in normal force was indicated for all angles of attack when either canopy was added to the body. Since C_N for the body alone remained constant as the sideslip angle was increased, the loss in normal force at the higher sideslip angle for either canopy-body configuration may have been due to local flow separation on the leeward side of the model induced by the addition of a canopy. At sideslip angles other than zero, the lateral-force coefficient (fig. 10(b)) for canopy 2 was larger than that for canopy 1. The addition of either canopy yielded a greater increase in lateral force with angle of attack.

The axial-force coefficient (fig. 10(c)) and the drag coefficient (fig. 10(d)) were increased by the addition of either canopy. The increase was greater at supersonic Mach numbers and amounted to as much as 0.12 in drag coefficient for canopy 2. In figure 10(d), it can be seen that the drag is always less for the flat windshield than for the vee windshield. The difference in drag coefficient due to windshield shape amounted to as much as 0.03. Unpublished data for these same models indicate similar measured drag differences at $M = 1.4$ and 2.0.

In the light of the transonic area rule (ref. 3), it appears that the larger drag of the vee-windshield model may be partially due to the greater rate of area growth between the 6-inch and 8.5-inch stations. (fig. 1(f)) for that model.

Windshield shape did not have an important effect on rolling moment (fig. 10(e)), pitching moment (fig. 10(f)), or yawing moment (fig. 10(g)). At sideslip angles of -4° and -8°, the rolling-moment coefficient was negative for the body alone as well as for either canopy-body combination. This was due to the drooped nose of the body which caused a greater frontal area to be presented below the roll axis. Since canopies 1 and 2 were mounted well forward and near the roll axis of the body, only a very slight positive rolling increment was produced by the canopies at $\beta = -8^\circ$, even though the lateral-force increments were relatively large. Nearly equal increments in pitching-moment coefficient (fig. 10(f)) were produced by both canopies at all angles of attack and sideslip. Since the increment in normal force at $\beta = 0^\circ$ and -4° was very near zero, the increase in pitching moment at these sideslip angles was produced by, essentially, a pure couple. At $\beta = -8^\circ$, the positive pitching-moment increment was maintained despite a negative increment in normal force. The yawing-moment increment due to adding either canopy (fig. 10(g)) decreased with increasing angle of attack, even though the lateral force increased.

Effect of Canopy Location

The variation of zero-lift drag with Mach number for the five models tested is shown in figure 11. By comparing the curves for canopy 3 (forward) and canopy 4 (rearward), it can be seen that the beginning of the transonic drag rise was delayed to a slightly higher Mach number and the supersonic drag was reduced slightly by placing the canopy in the forward position. It can also be seen, by comparing the curves for canopies 1 and 2 with those for canopies 3 and 4, that reducing the size of the canopies improves the area distribution (fig. 1(f)) and yields a considerable reduction in the drag at low supersonic speeds.

The basic data for canopies 3 and 4 are presented in figures 6 and 7. Examination of these data indicates that either canopy location produced the same normal-force and lateral-force characteristics within the accuracy of the data. The rolling-moment coefficient also showed no significant change due to canopy location. The positive pitching moment was slightly greater for the forward canopy except near $M = 0.99$ and $\alpha = 10^\circ$ where the rearward canopy exhibited a slightly greater positive pitching tendency. The yawing moment was essentially the same for both canopies except near $M = 0.99$ and $\beta = -8^\circ$, where a slight increase was indicated for the rearward canopy.

[redacted]

CONCLUSIONS

Aerodynamic data have been obtained for four canopies mounted on a fuselage forebody. Two of the canopies had the same shape and size rearward of the windshield but one had a "flat" and the other a "vee" windshield. The remaining two canopies were located at different body stations and were geometrically similar. They had a smaller maximum cross-sectional area than the first two. The data obtained indicated that:

1. The drag of the flat-windshield canopy model used in this investigation was consistently lower than that of the similar vee-windshield model through a Mach number range from 0.80 to 1.13, an angle-of-attack range from 0° to 10°, and an angle-of-sideslip range from -8° to 8°.

2. Of the remaining forces and moments, only the lateral force was significantly affected by windshield shape, the vee-shaped windshield causing increased lateral force.

3. Little effect of canopy location was found for the canopy-body configurations used in this investigation.

Langley Aeronautical Laboratory,
National Advisory Committee for Aeronautics,
Langley Field, Va., June 20, 1955.

REFERENCES

1. Wright, Ray H., and Ritchie, Virgil S.: Characteristics of a Transonic Test Section With Various Slot Shapes in the Langley 8-Foot High-Speed Tunnel. NACA RM L51H10, 1951.

2. Ritchie, Virgil S., and Pearson, Albin O.: Calibration of the Slotted Test Section of the Langley 8-Foot Transonic Tunnel and Preliminary Experimental Investigation of Boundary-Reflected Disturbances. NACA RM L51K14, 1952.

3. Whitcomb, Richard T.: A Study of the Zero-Lift Drag-Rise Characteristics of Wing-Body Combinations Near the Speed of Sound. NACA RM L52H08, 1952.

[redacted]

BODY DIMENSIONS			
x	a	b	z
0	0	0	1.000
.250	.073	.058	.973
.500	.144	.115	.945
.750	.214	.171	.917
1.000	.283	.226	.896
1.250	.351	.281	.863
1.500	.418	.334	.837
1.750	.483	.386	.811
2.000	.548	.438	.785
2.250	.611	.489	.760
2.500	.674	.539	.735
3.750	.969	.775	.617
5.000	1.237	.990	.510
6.250	1.479	1.183	.413
7.500	1.695	1.356	.326
8.750	1.885	1.508	.250
10.000	2.049	1.639	.183
11.250	2.187	1.750	.127
12.500	2.300	1.840	.081
13.750	2.388	1.910	.046
15.000	2.450	1.960	.020
16.250	2.480	1.990	.005
17.500	2.500	2.000	.000
	↓	↓	↓
25.000	2.500	2.000	.000

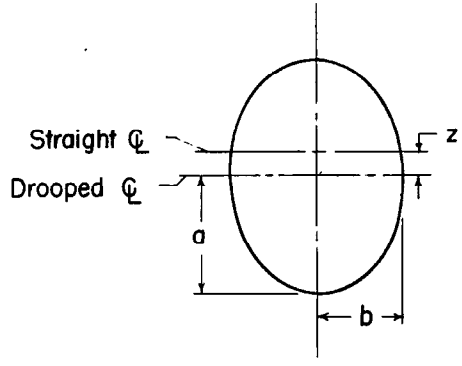

Section A-A

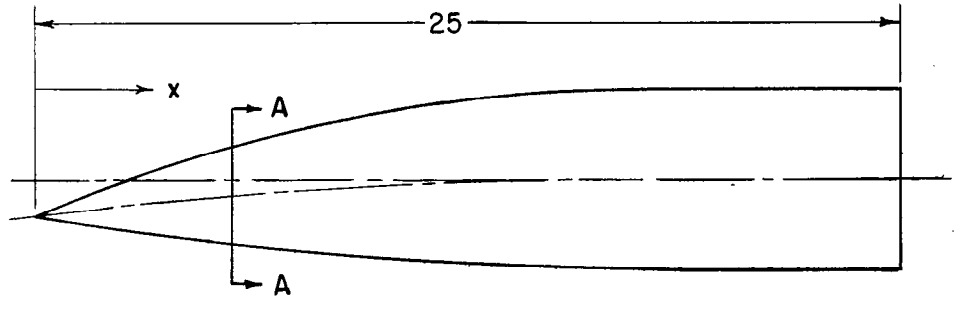

(a) Body.

Figure 1.- Model details. All dimensions are in inches.

CANOPY FACE					
x = 3.750		x = 5.000		x = 6.250	
v	u	v	u	v	u
0.000	0.358	0.000	1.227	0.000	2.117
	↓		↓		↓
.350	.358	.350	1.227	.350	2.117
.438	.244	.438	1.130	.438	2.015
.563	.050	.563	.956	.563	1.814
		.688	.694	.688	1.562
		.813	.330	.813	1.230
		.878	.120		
				.938	.762
				1.063	.271

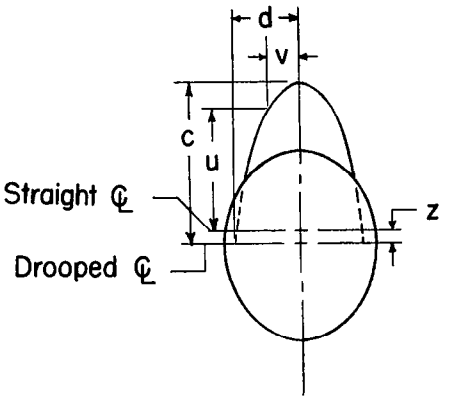

CANOPY BODY		
x	c	d
7.500	3.096	1.238
8.750	3.175	1.270
10.000	3.148	1.259
11.250	3.077	1.231
12.500	2.961	1.184
13.750	2.811	1.124
15.000	2.655	1.062
16.250	2.480	.992

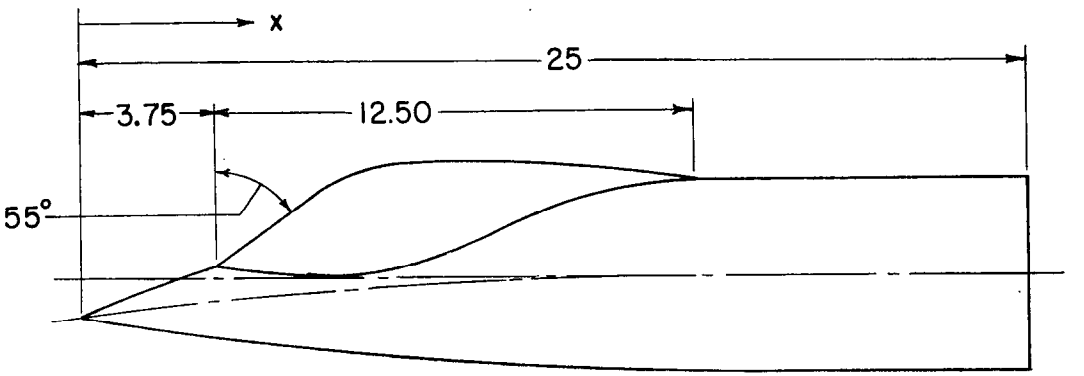

(b) Canopy 1.

Figure 1.- Continued.

CANOPY BODY		
x	c	d
3.750	0.969	
5.000	1.737	
6.250	2.516	1.006
7.500	3.096	1.238
8.750	3.175	1.270
10.000	3.148	1.259
11.250	3.077	1.231
12.500	2.961	1.184
13.750	2.811	1.124
15.000	2.655	1.062
16.250	2.480	.992

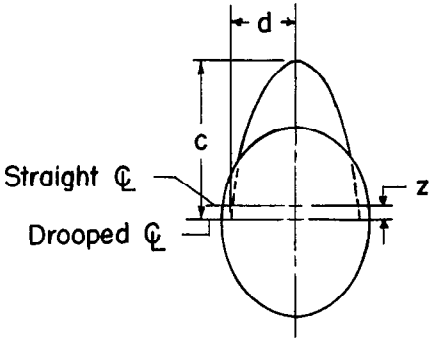

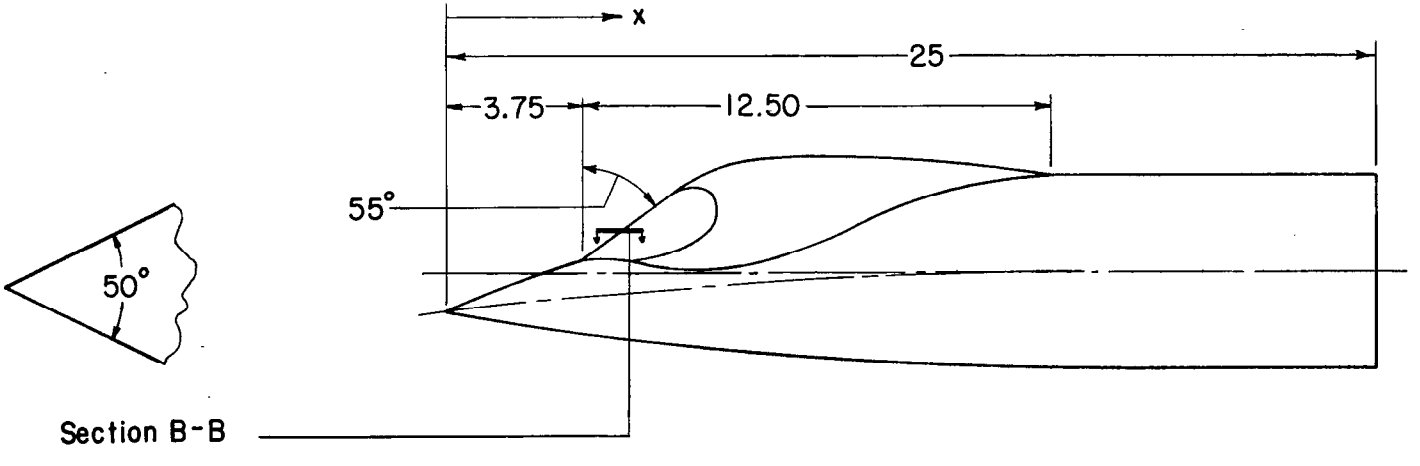

(c) Canopy 2.

Figure 1.- Continued.

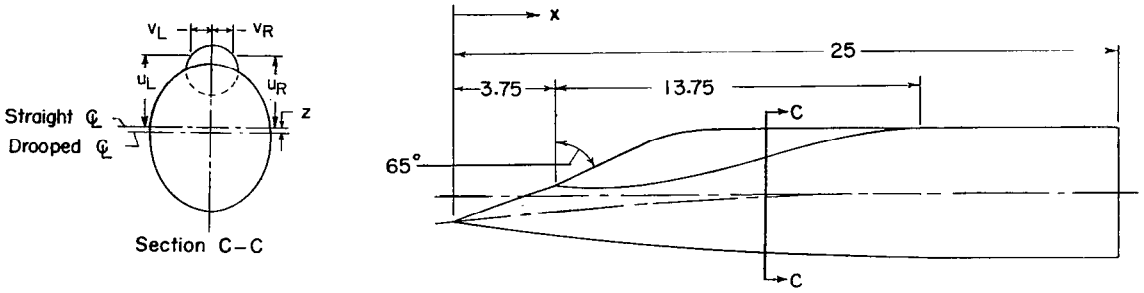

MEASURED COORDINATES									
x	v_L	u_L	v_R	u_R	x	v_L	u_L	v_R	u_R
3.816	0	0.352	0	0.352	10.066	0	2.476	0	2.476
	.350	.322	.350	.352		.390	2.385	.390	2.382
	.425	.244	.425	.268		.533	2.293	.533	2.288
	.475	.163	.475	.187		.629	2.198	.629	2.195
	.508	.109	.508	.132		.698	2.101	.690	2.098
5.066	0	.945	0	.945		.748	2.010	.748	2.006
	.350	.919	.350	.945		.782	1.937	.782	1.916
	.475	.803	.475	.820		.802	1.886	.802	1.832
	.600	.594	.600	.641		.809	1.867	.809	1.795
	.675	.407	.675	.454		.863	1.545	.805	1.552
	.684	.393	.684	.402	11.316	0	2.476	0	2.476
6.316	0	1.551	0	1.551		.370	2.378	.370	2.380
	.350	1.530	.350	1.541		.503	2.284	.503	2.283
	.475	1.435	.475	1.430		.591	2.185	.591	2.187
	.600	1.280	.600	1.276		.653	2.095	.653	2.086
	.725	1.052	.725	1.059		.695	2.021	.695	1.991
	.803	.693	.796	.693		.721	1.968	.721	1.905
7.566	0	2.118	0	2.118		.771	1.809	.735	1.811
	.381	2.036	.381	2.033	12.566	0	2.475	0	2.475
	.540	1.945	.540	1.935		.348	2.371	.348	2.381
	.647	1.851	.647	1.824		.472	2.269	.472	2.283
	.724	1.757	.724	1.708		.552	2.172	.552	2.174
	.782	1.653	.782	1.592		.615	2.054	.615	2.034
	.823	1.554	.823	1.489	13.816	0	2.477	0	2.477
	.851	1.467	.851	1.388		.326	2.373	.326	2.383
	.866	1.403	.866	---		.439	2.274	.439	2.284
	.860	.997	.829	1.000		.471	2.229	.483	2.223
8.816	0	2.411	0	2.411	15.066	0	2.485	0	2.485
	.212	2.391	.212	2.384		.332	2.351	.345	2.359
	.447	2.310	.447	2.292	16.316	0	2.492	0	2.492
	.578	2.226	.578	2.198		.193	2.438	.222	2.433
	.670	2.140	.670	2.103					
	.737	2.058	.737	2.005					
	.786	1.974	.786	1.903					
	.819	1.900	.819	1.810					
	.840	1.841	.840	1.749					
	.849	1.810	.849	1.745					
	.878	1.283	.830	1.290					

NOTE: Last entry at each x-station gives canopy-body intersection.

(d) Canopy 3.

Figure 1.- Continued.

CANOPY FACE			
x = 7.500		x = 8.750	
v	u	v	u
0	1.395	0	1.952
	↓		↓
	↓		↓
	↓		↓
.350	1.395	.350	1.952
.375	1.379	.400	1.922
.400	1.361	.450	1.880
.425	1.351	.500	1.823
.450	1.320	.550	1.750
.475	1.297	.600	1.643
.500	1.274	.625	1.575
.525	1.249	.650	1.500
.550	1.229	.673	1.425

CANOPY BODY		
x	h	r
10.000	2.514	0.772
11.250	2.833	.758
12.500	2.882	.738
13.750	2.827	.683
15.000	2.773	.629
16.250	2.718	.574
17.500	2.664	.520
19.375	2.582	.438
21.250	2.500	.356

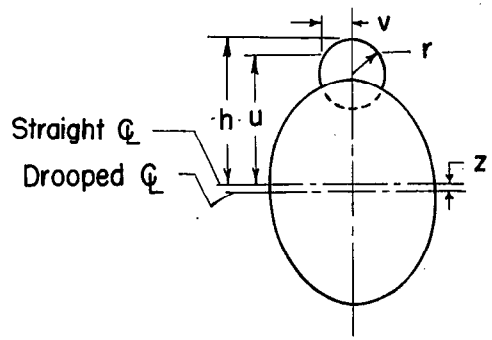

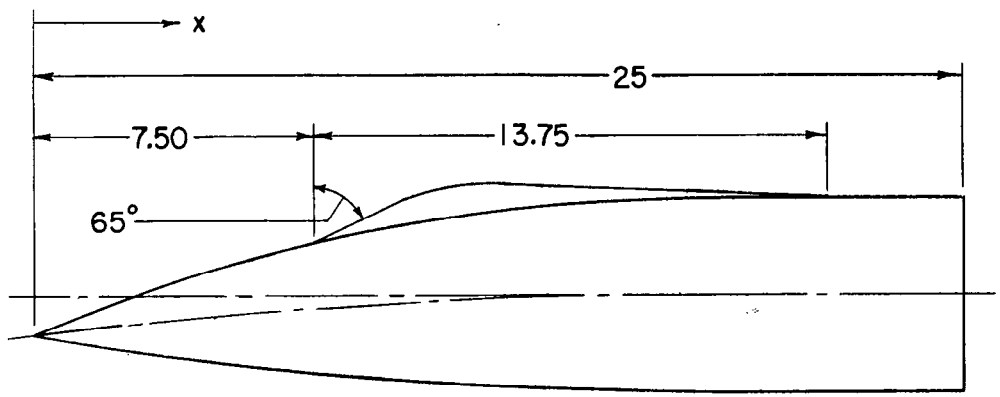

(e) Canopy 4.

Figure 1.- Continued.

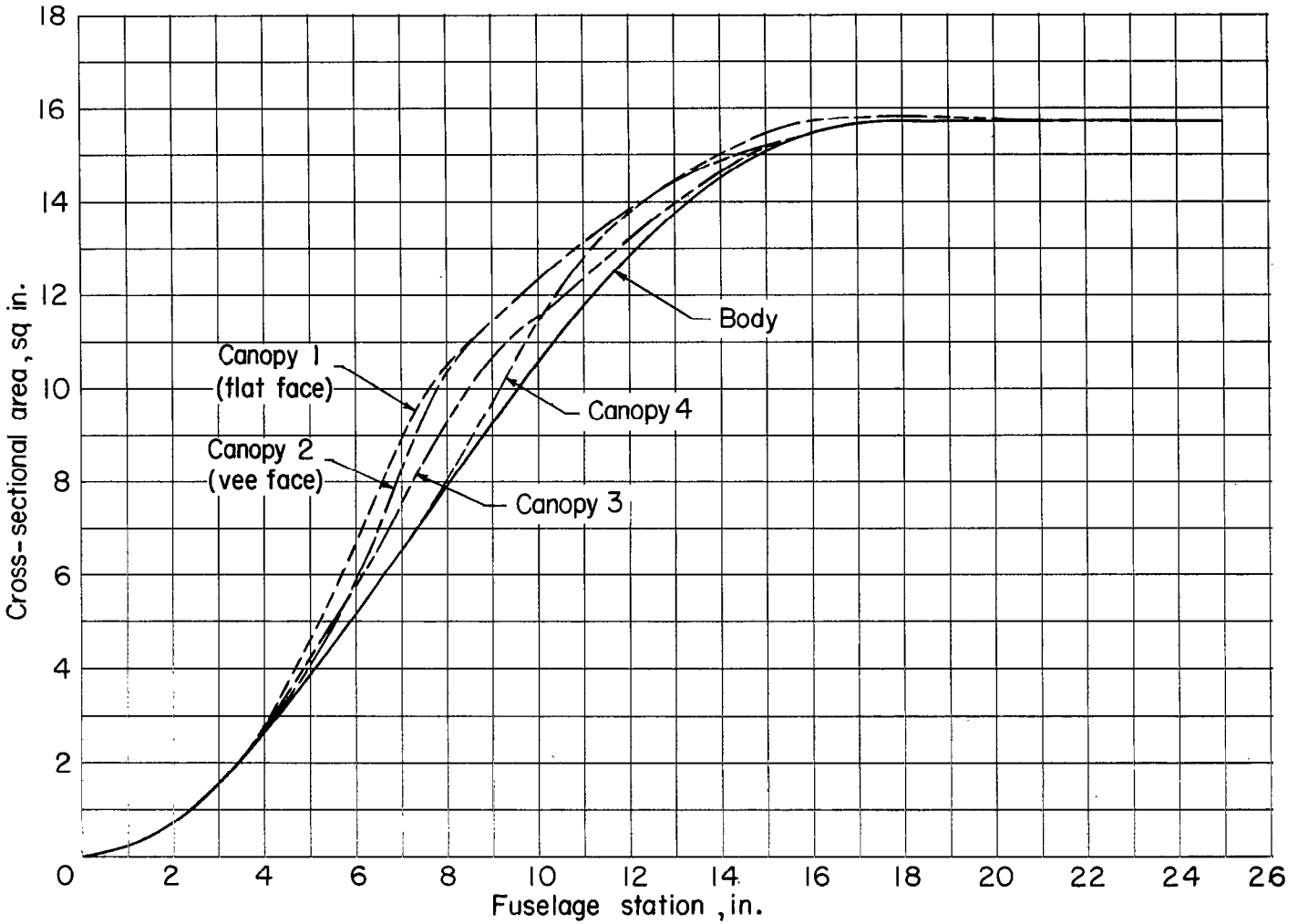

(f) Area distributions.

Figure 1.- Concluded.

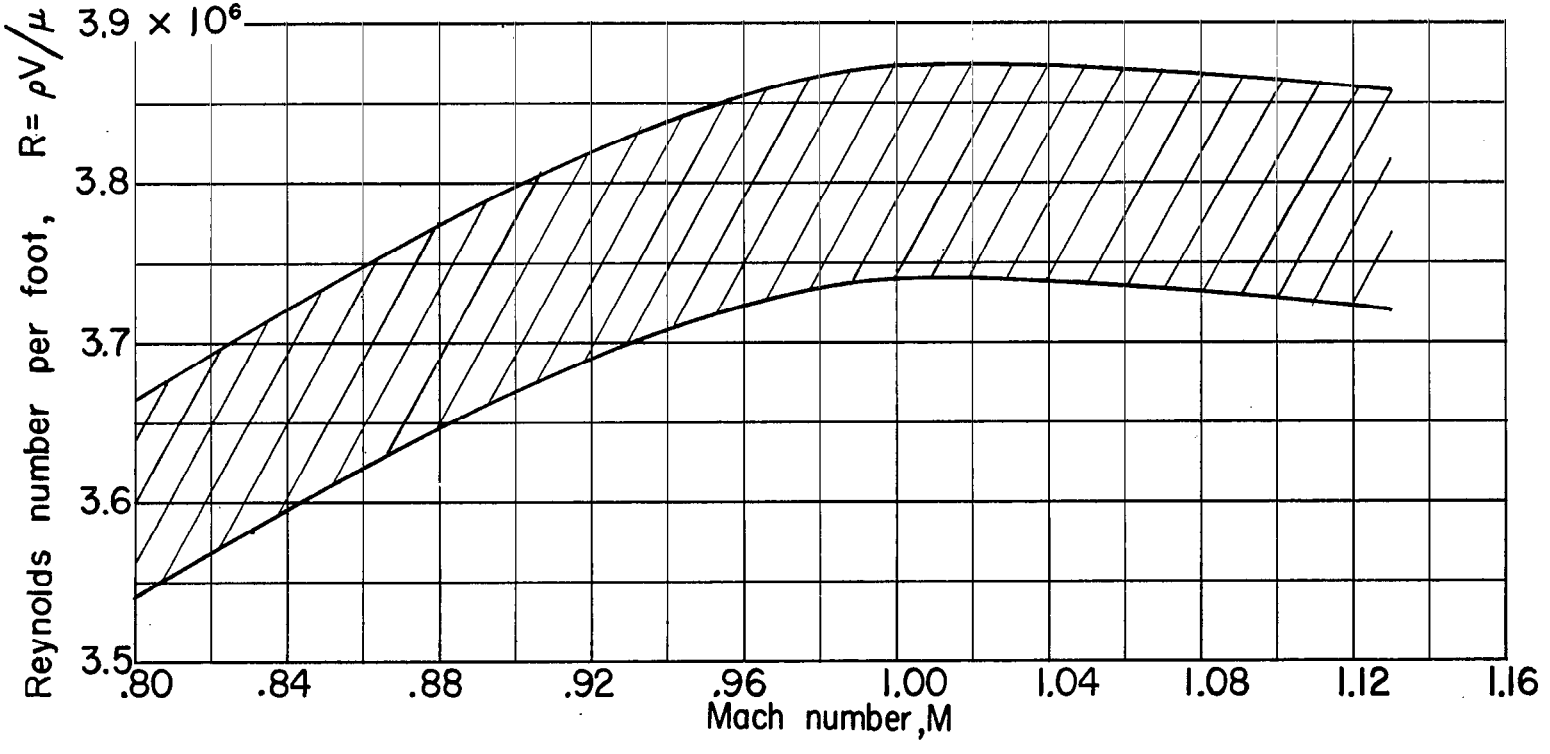

Figure 2.- Variation of Reynolds number with Mach number.

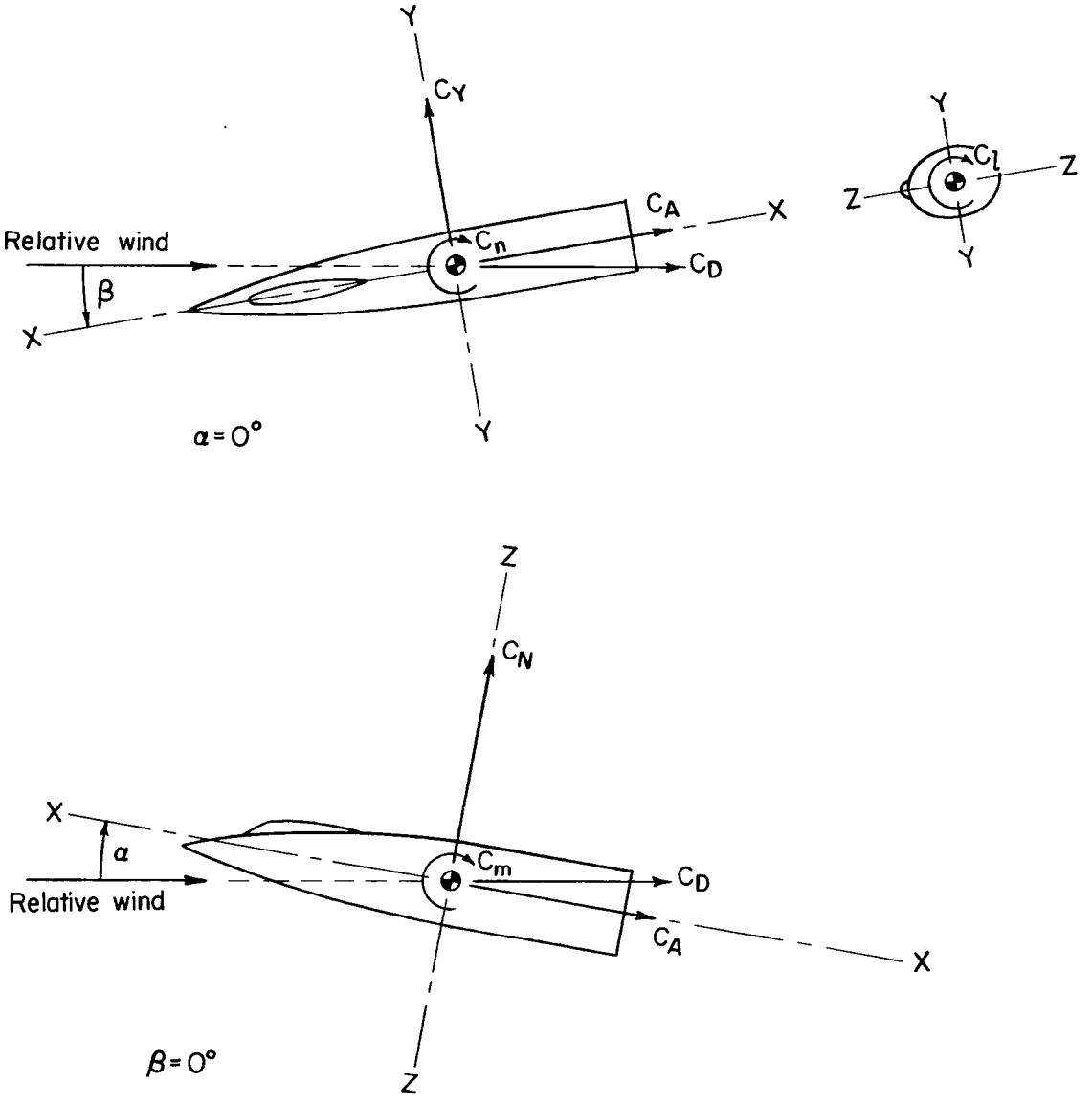

Figure 3.- Body-axis system used. Positive forces, moments, and angles are indicated by arrows.

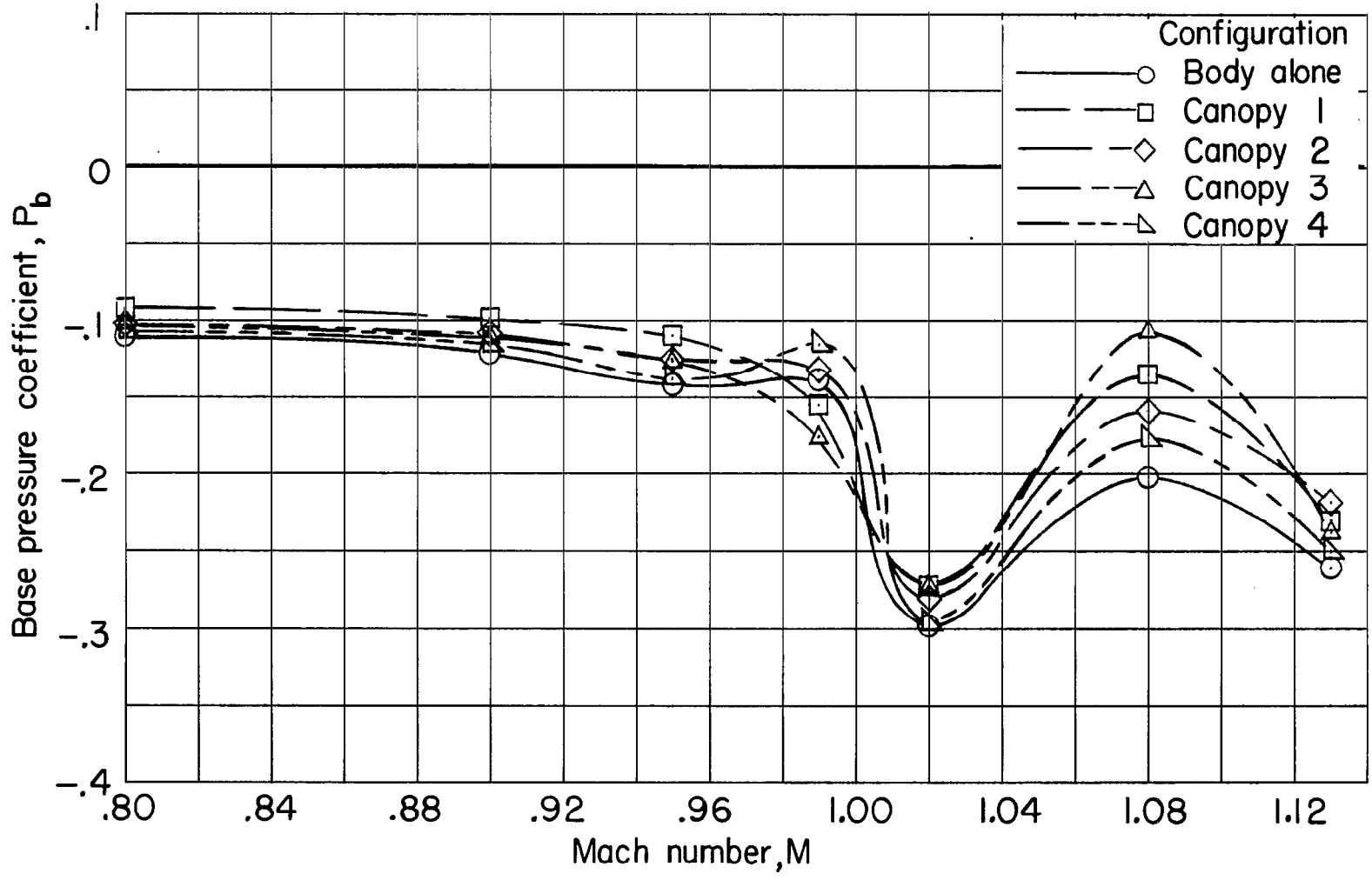

Figure 4.- Variation of base pressure coefficient with Mach number. $\beta = 0^\circ$; $\alpha = 0^\circ$ (approx.).

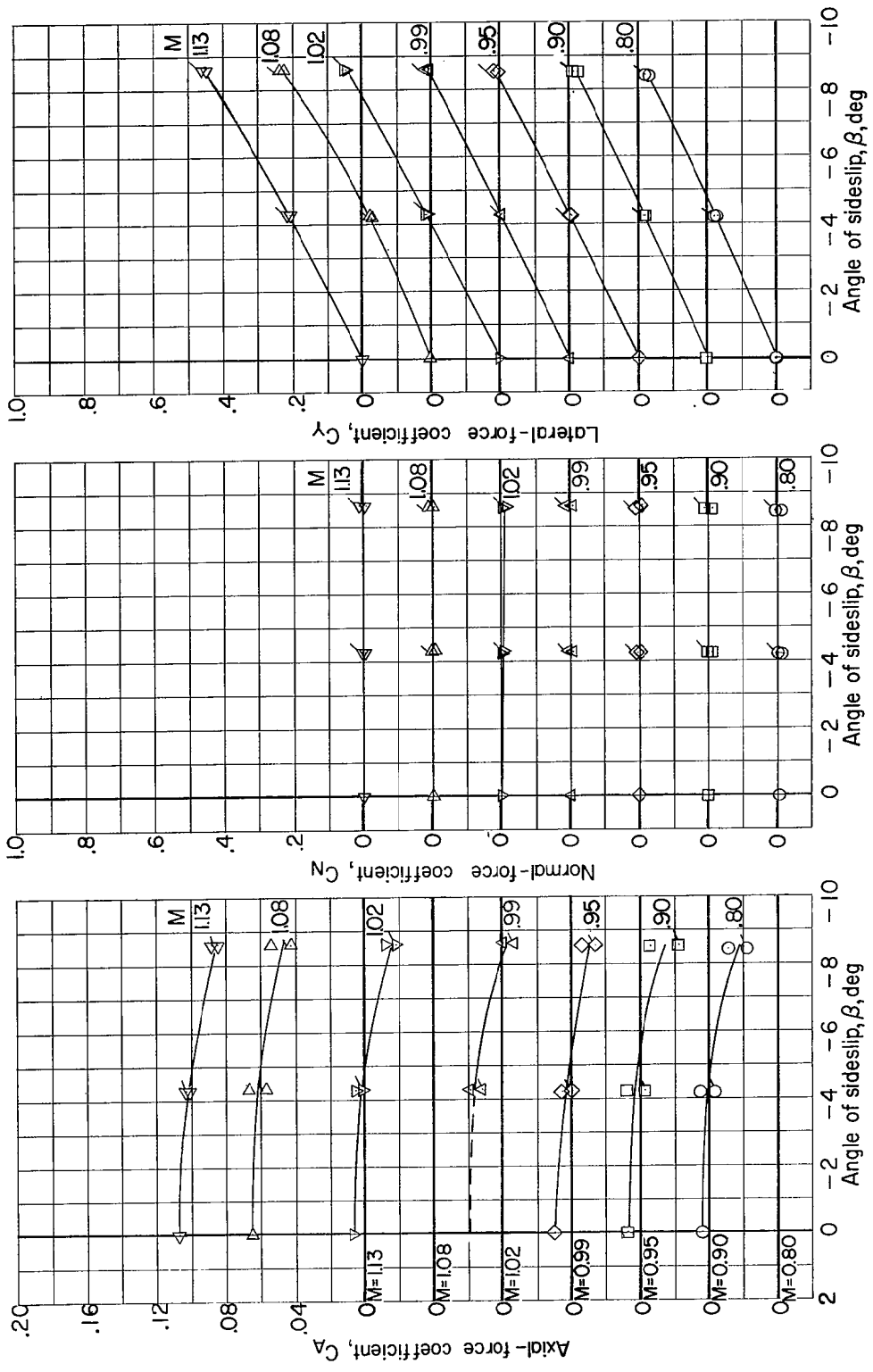
Axial-force coefficient, C_A
Normal-force coefficient, C_N
Lateral-force coefficient, C_Y
Angle of sideslip, β, deg
M
1.13
1.08
1.02
.99
.95
.90
.80
M=1.13
M=1.08
M=1.02
M=0.99
M=0.95
M=0.90
M=0.80

[redacted]

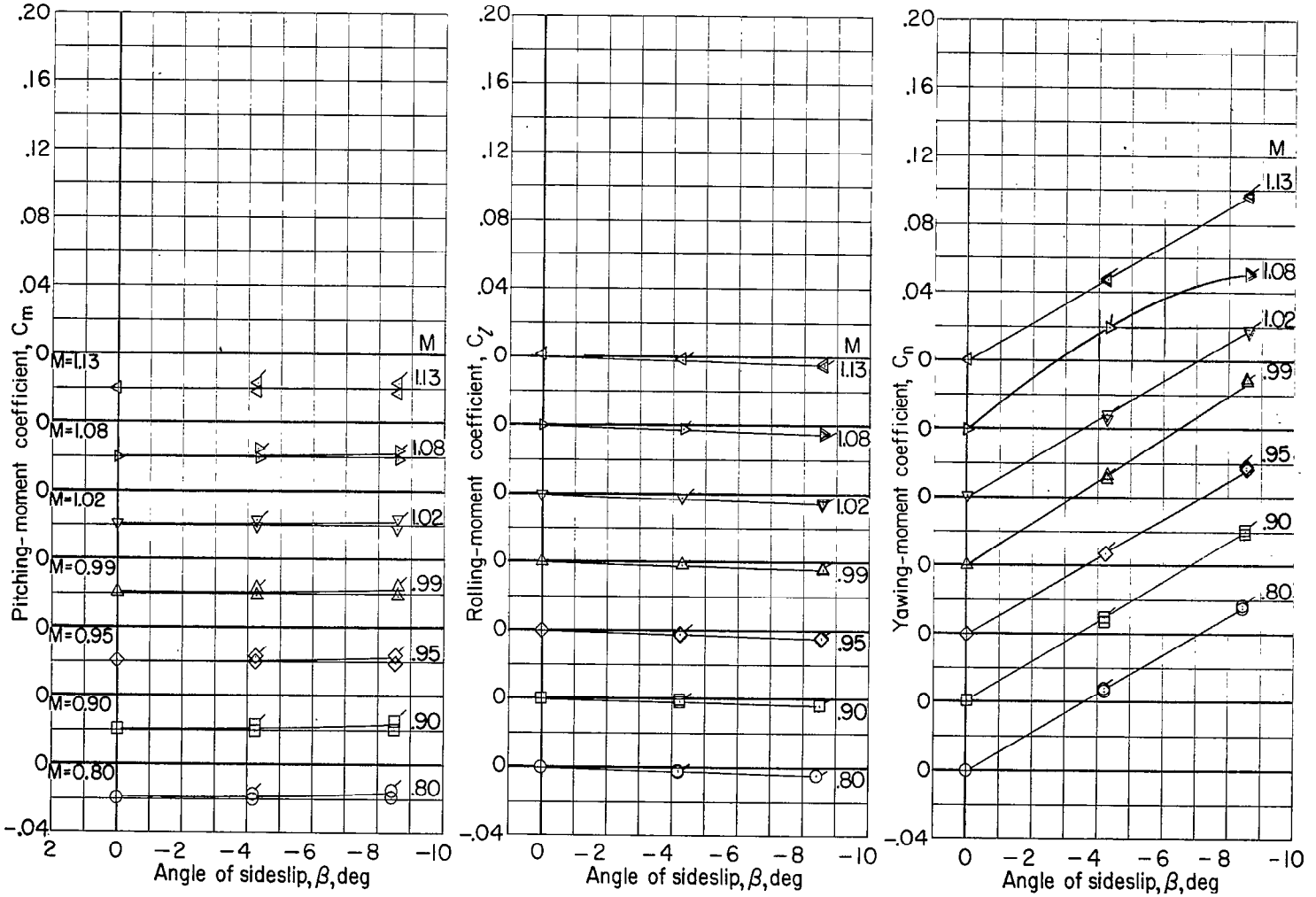

(a) $\alpha = -0.1^\circ$.

Figure 5.- Aerodynamic coefficients for body alone. (Flagged symbols indicate data at positive sideslip angles.)

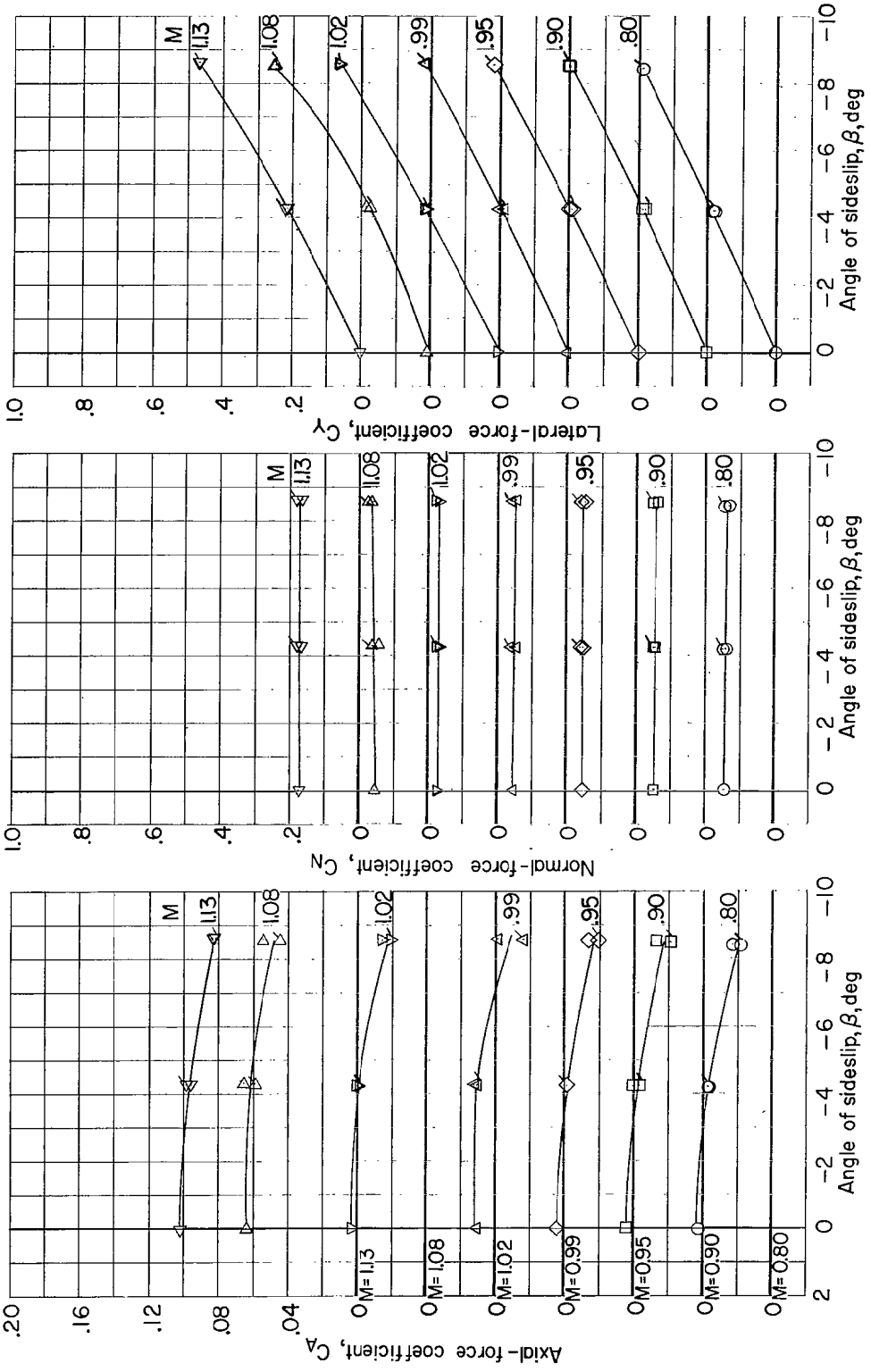
Axial-force coefficient, C_A
Normal-force coefficient, C_N
Lateral-force coefficient, C_Y
Angle of sideslip, β, deg
M
1.13
1.08
1.02
.99
.95
.90
.80
$M=1.13$
$M=1.08$
$M=1.02$
$M=0.99$
$M=0.95$
$M=0.90$
$M=0.80$

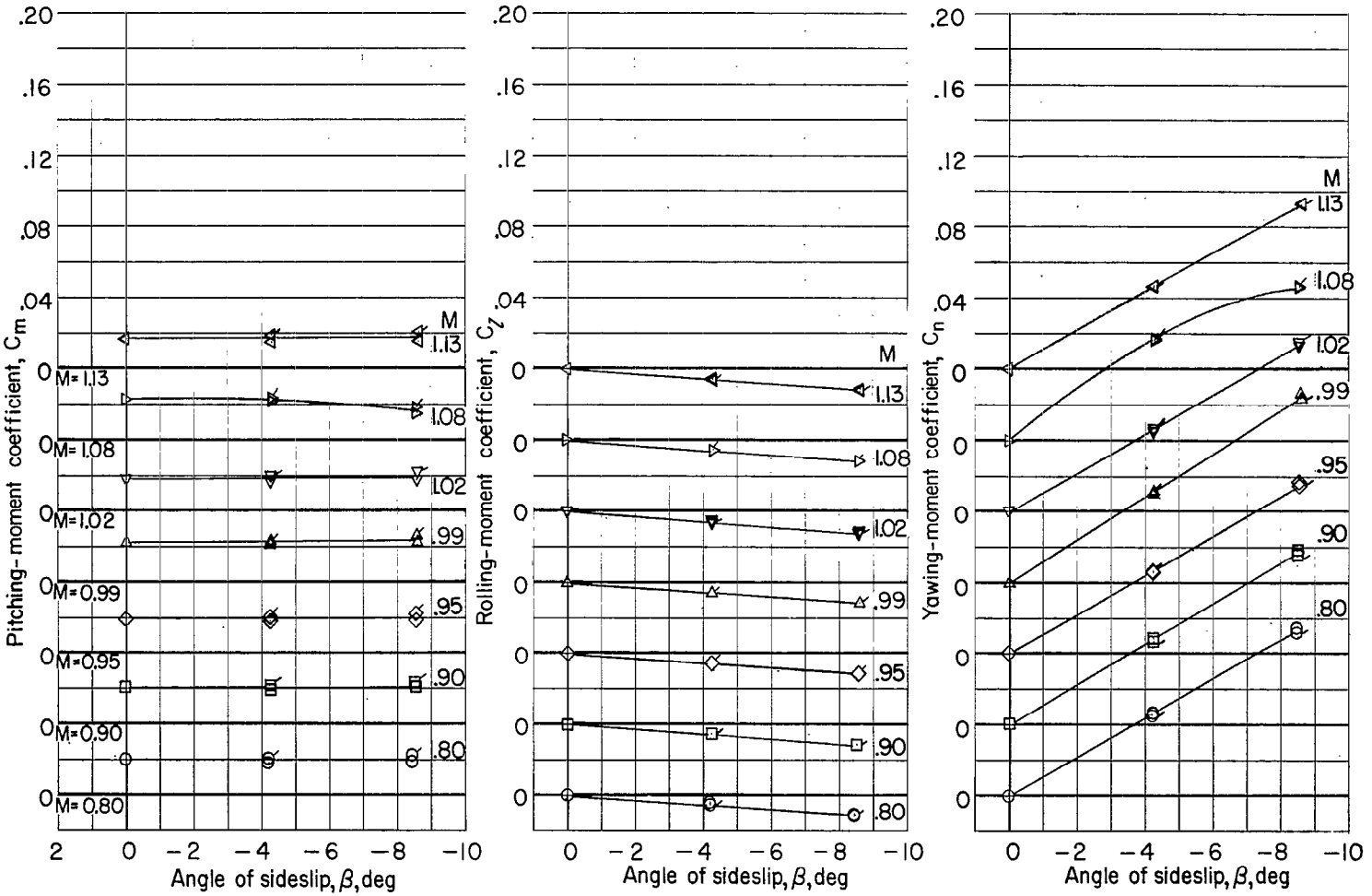

(b) $\alpha = 5.1^\circ$.

Figure 5.- Continued.

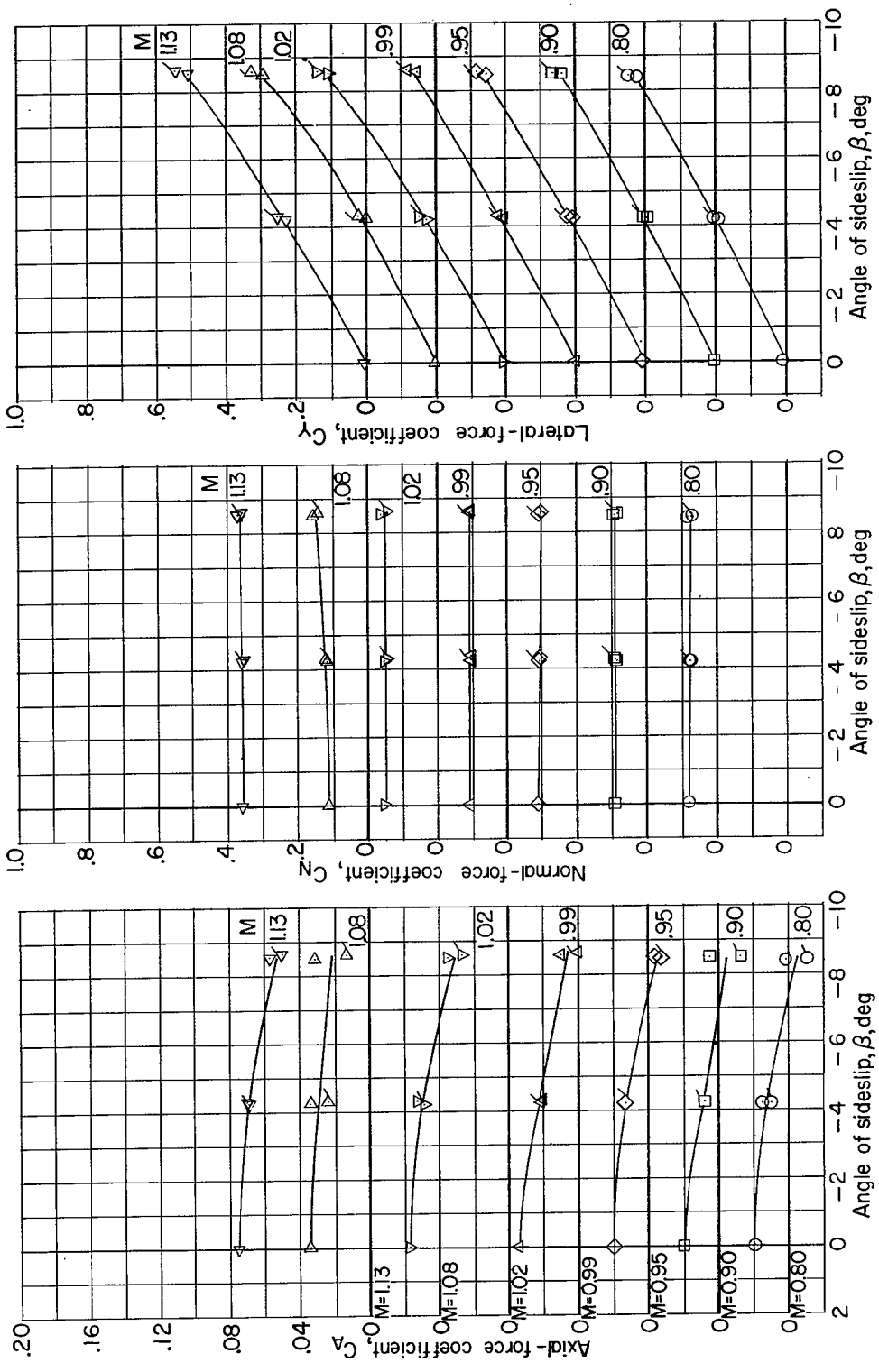
Axial-force coefficient, C_A
Normal-force coefficient, C_N
Lateral-force coefficient, C_Y
Angle of sideslip, β, deg
M
1.13
1.08
1.02
.99
.95
.90
.80
M=1.13
M=1.08
M=1.02
M=0.99
M=0.95
M=0.90
M=0.80

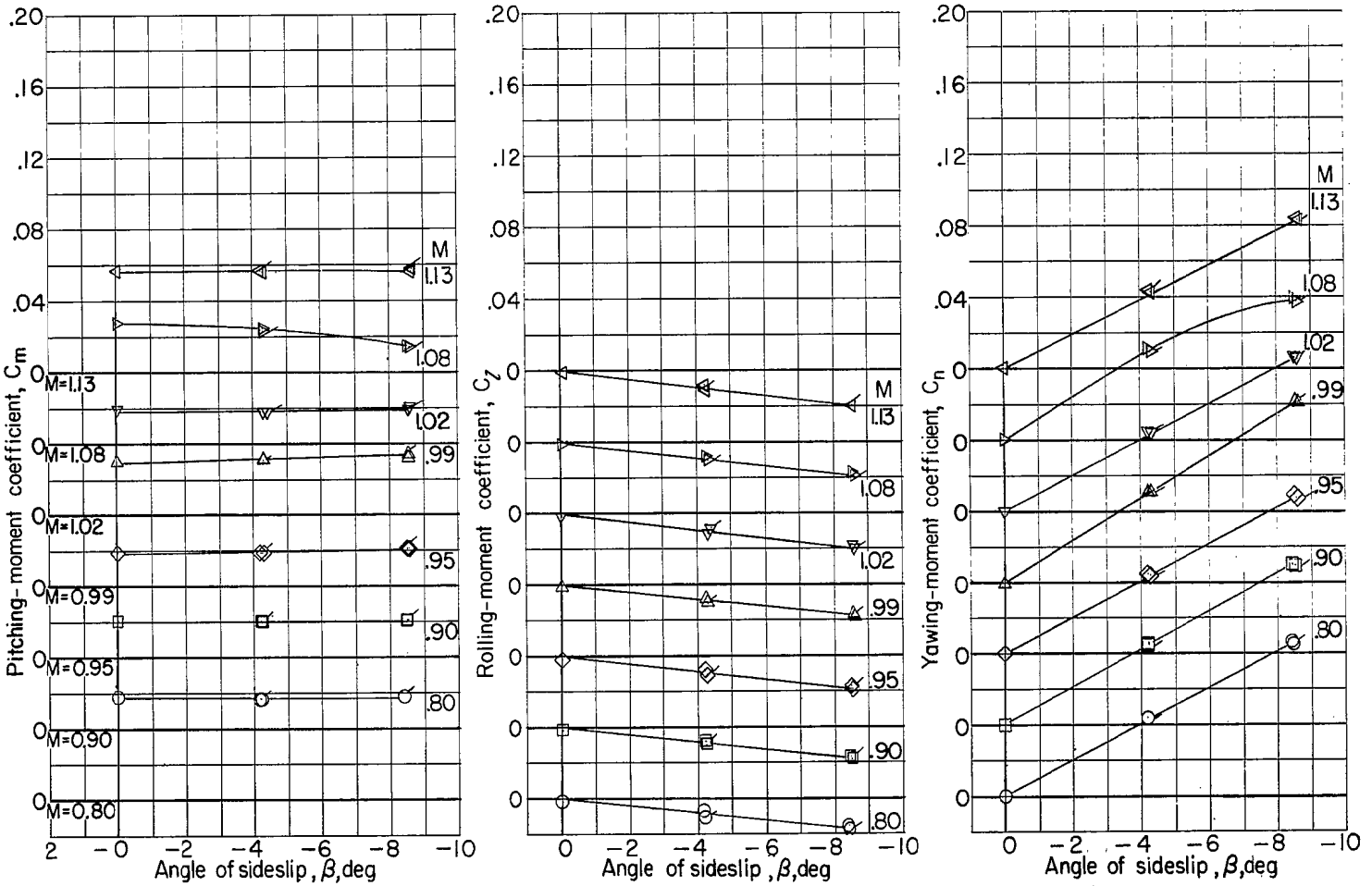

(c) $\alpha = 10.2^{\circ}$.

Figure 5.- Concluded.

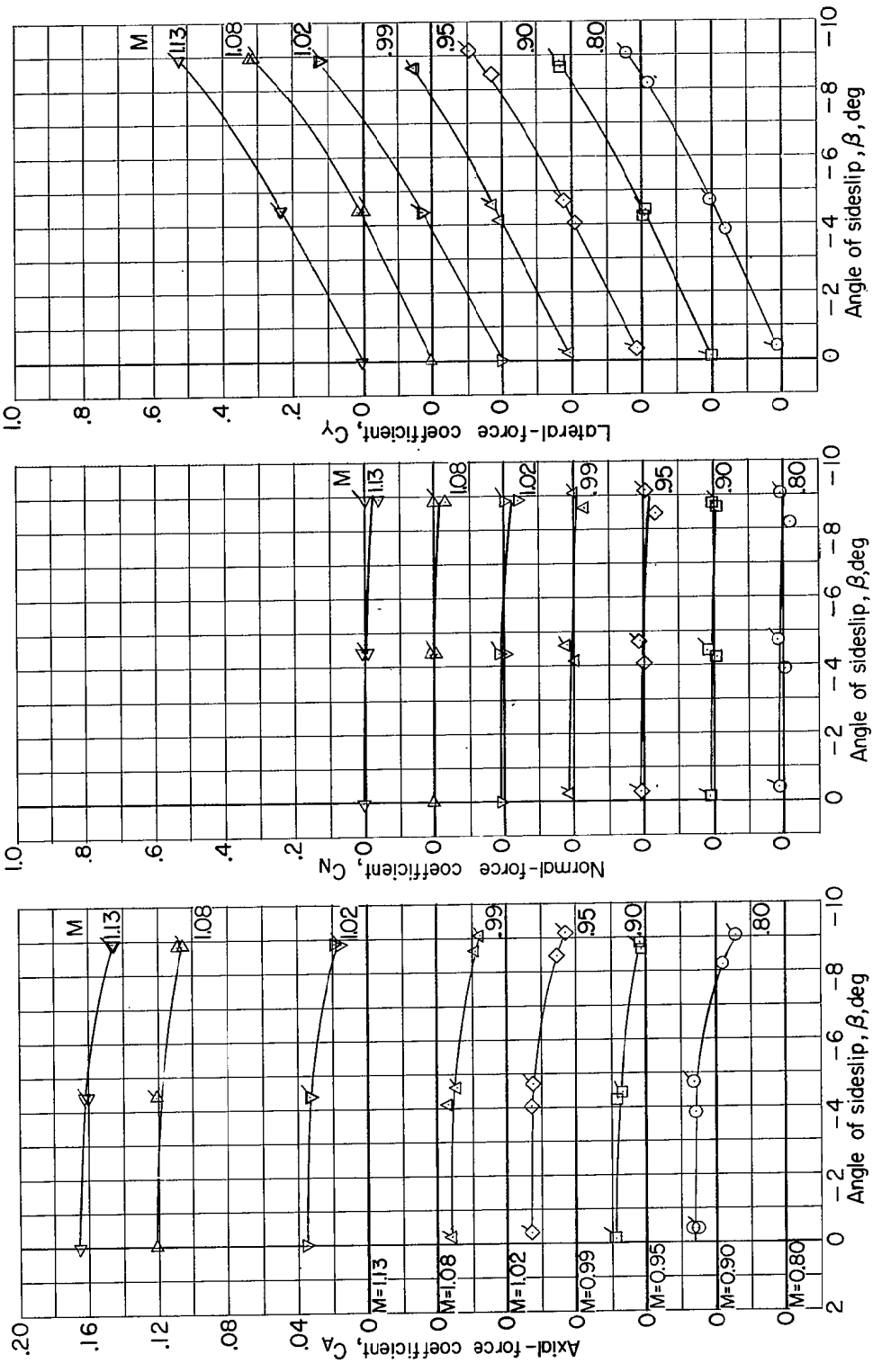
Axial-force coefficient, C_A
Normal-force coefficient, C_N
Lateral-force coefficient, C_Y
Angle of sideslip, β, deg
M
1.13
1.08
1.02
.99
.95
.90
.80
M=1.13
M=1.08
M=1.02
M=0.99
M=0.95
M=0.90
M=0.80

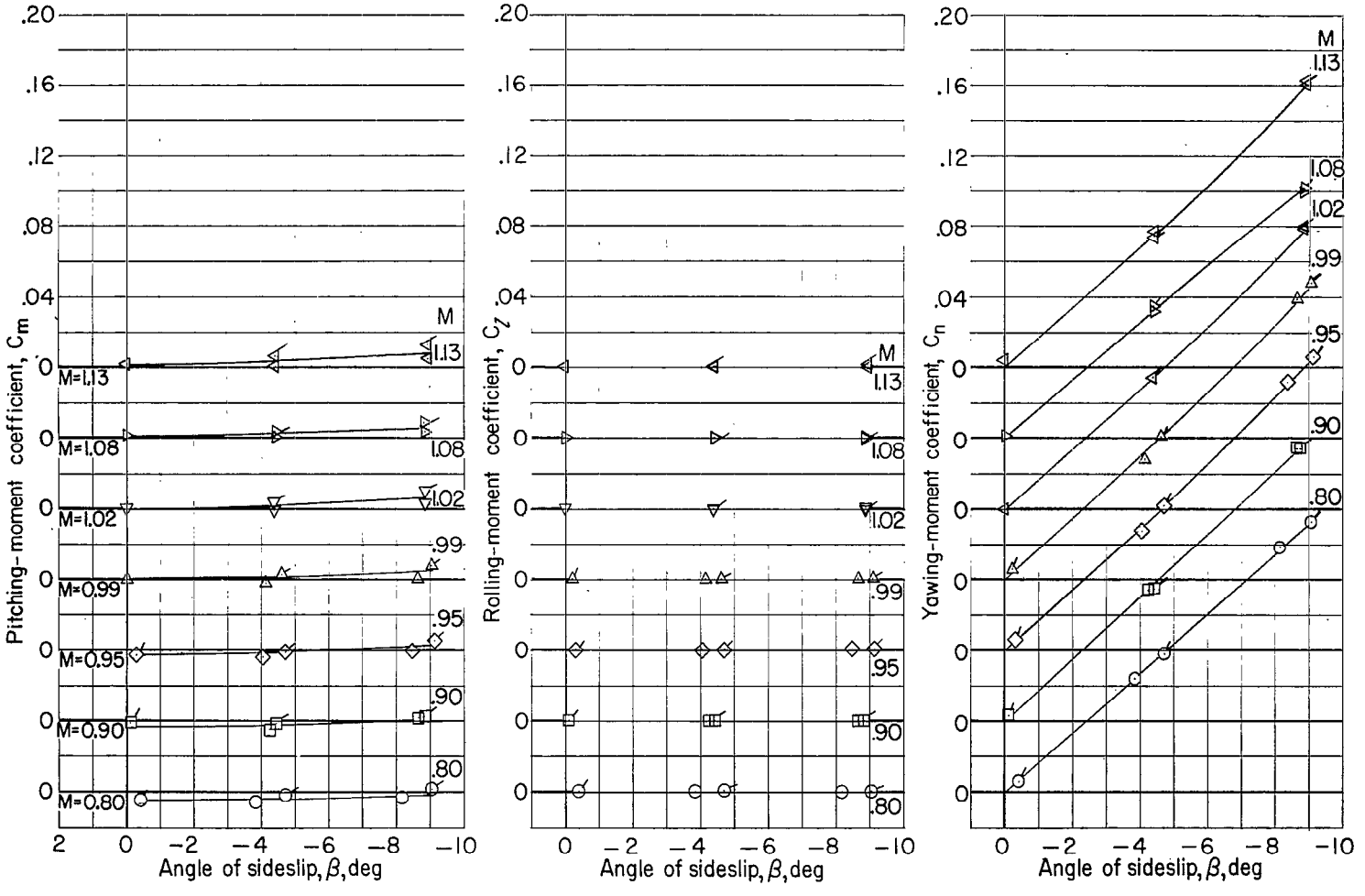

(a) $\alpha = 0^\circ$.

Figure 6.- Aerodynamic coefficients for canopy 1. (Flagged symbols indicate data at positive sideslip angles.)

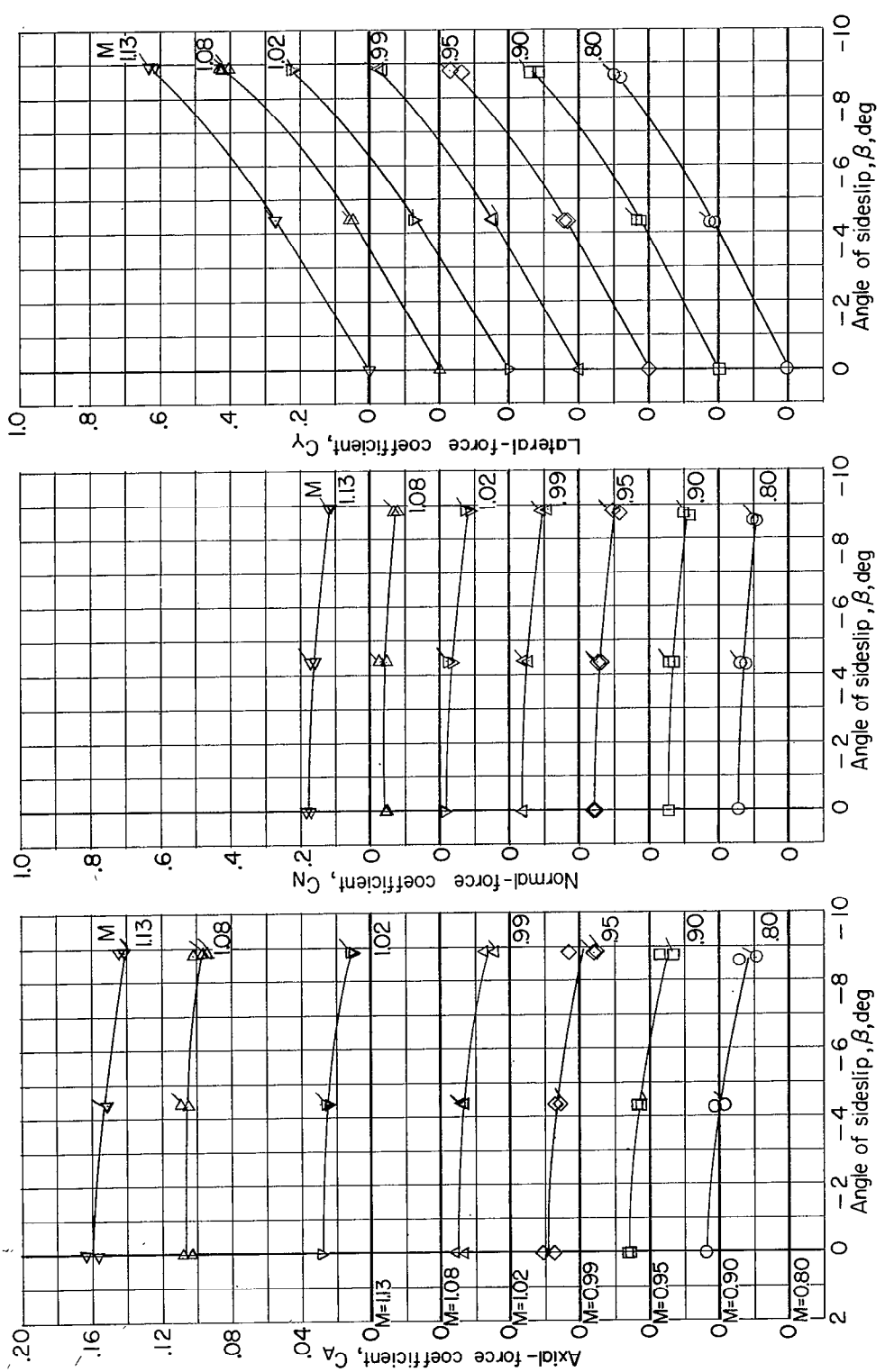
Axial-force coefficient, C_A
Normal-force coefficient, C_N
Lateral-force coefficient, C_Y
Angle of sideslip, β, deg
M
1.13
1.08
1.02
.99
.95
.90
.80
M=1.13
M=1.08
M=1.02
M=0.99
M=0.95
M=0.90
M=0.80

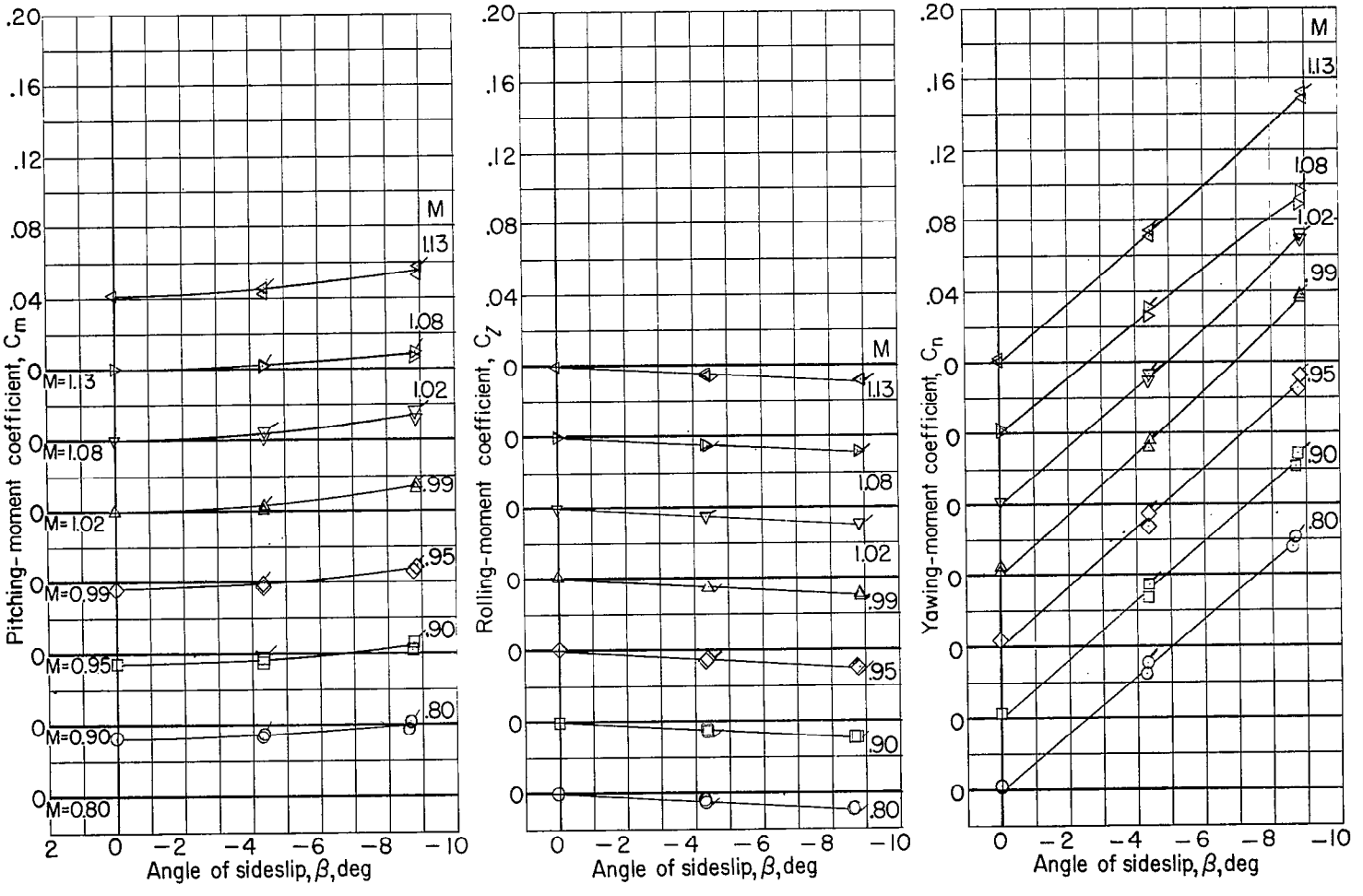

(b) $\alpha = 5.1^\circ$.

Figure 6.- Continued.

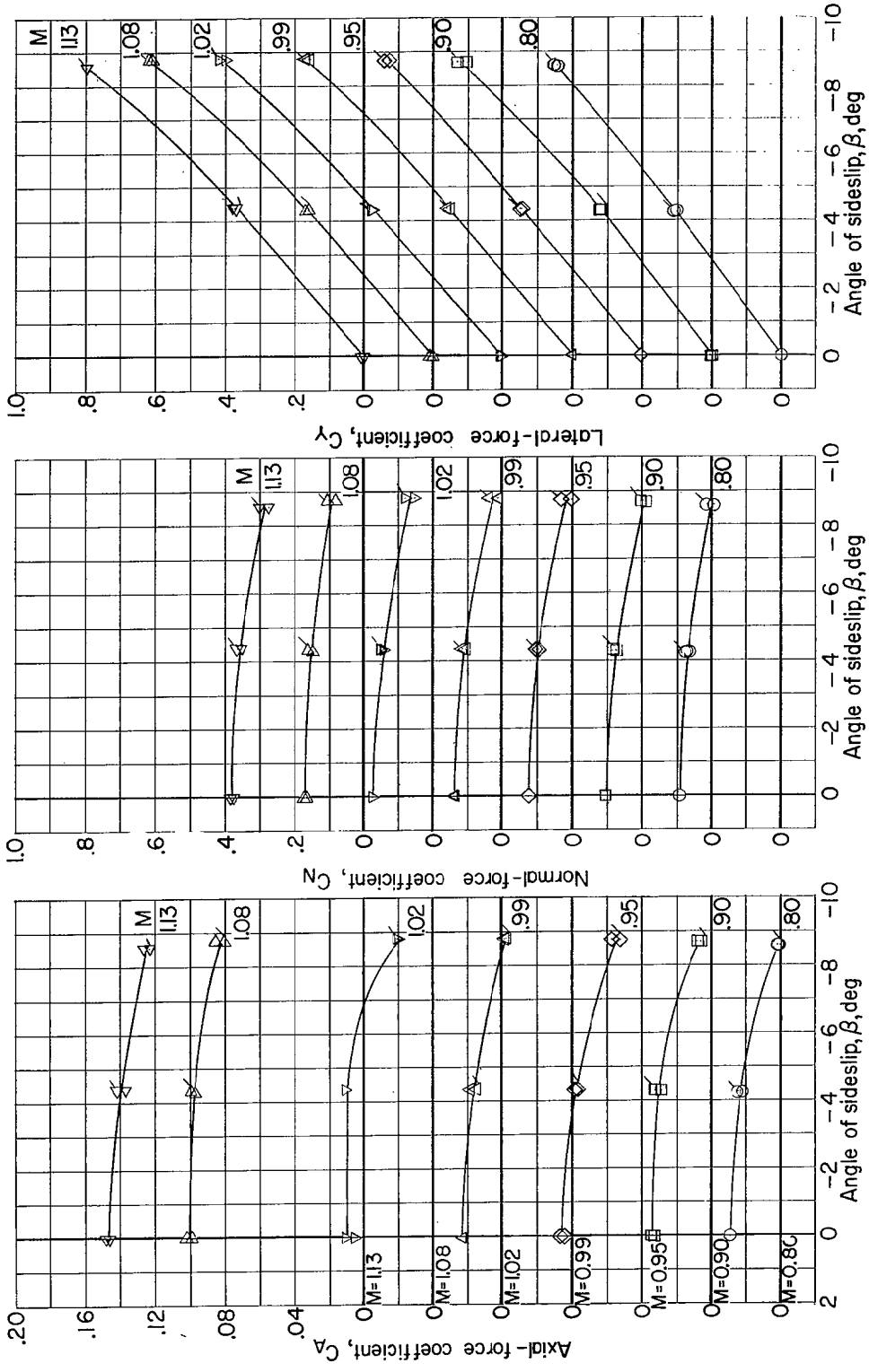
Axial-force coefficient, C_A
Normal-force coefficient, C_N
Lateral-force coefficient, C_Y
Angle of sideslip, β, deg
M
1.13
1.08
1.02
.99
.95
.90
.80
M=1.13
M=1.08
M=1.02
M=0.99
M=0.95
M=0.90
M=0.80

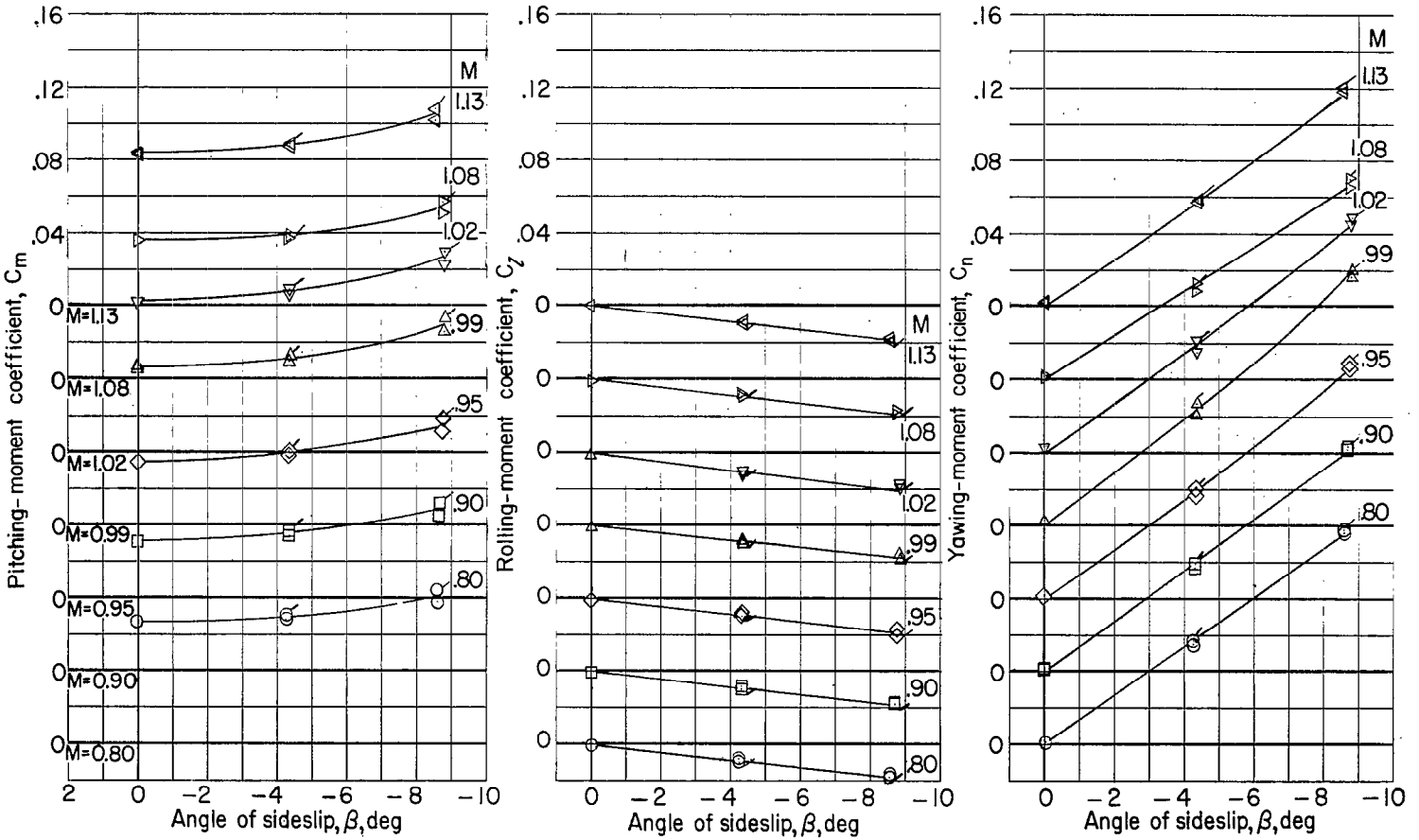

(c) $\alpha = 10.3^{\circ}$.

Figure 6.- Concluded.

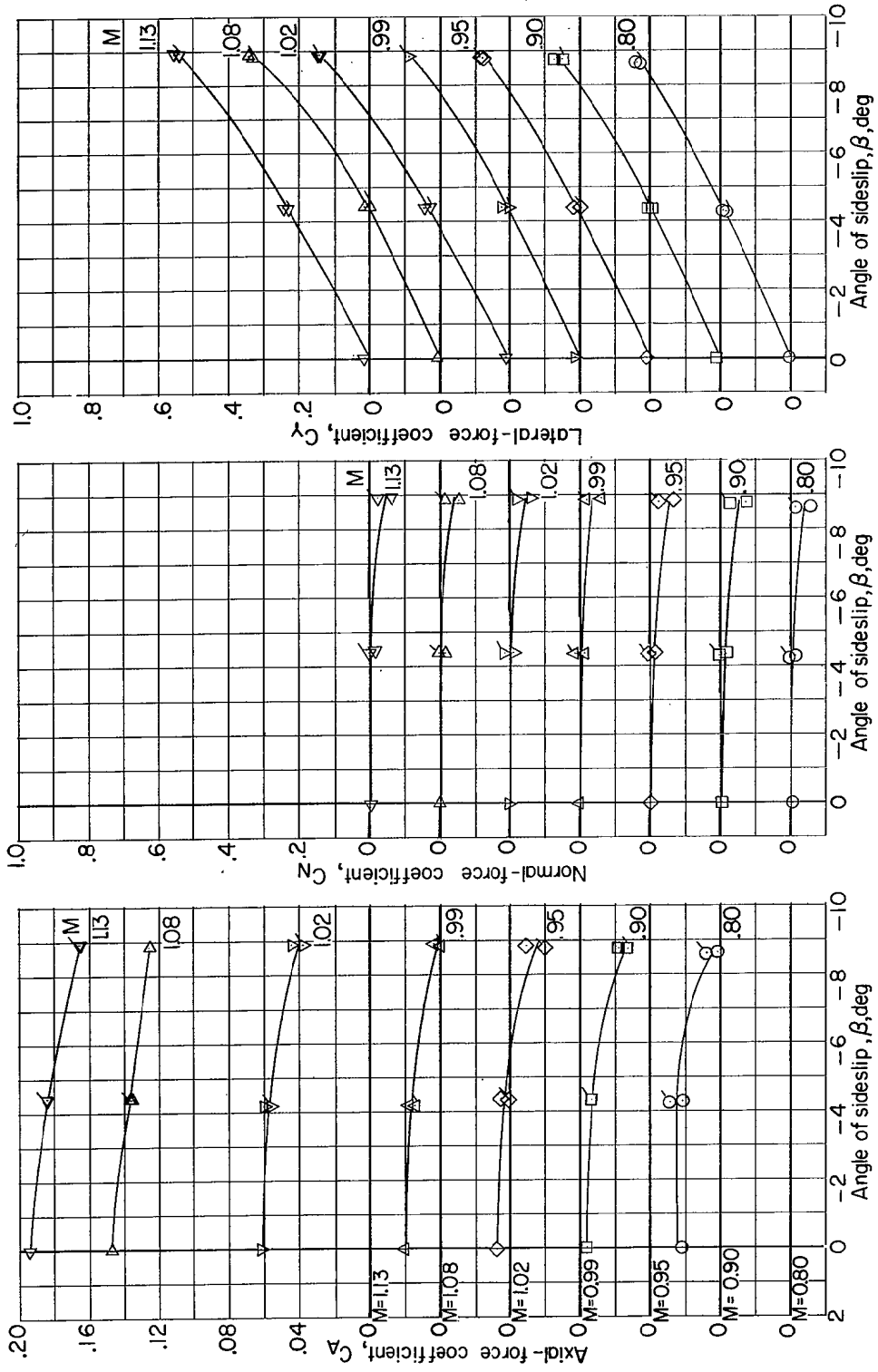
Axial-force coefficient, C_A
Normal-force coefficient, C_N
Lateral-force coefficient, C_Y
Angle of sideslip, β, deg
M
1.13
1.08
1.02
.99
.95
.90
.80
M=1.13
M=1.08
M=1.02
M=0.99
M=0.95
M=0.90
M=0.80

[redacted]

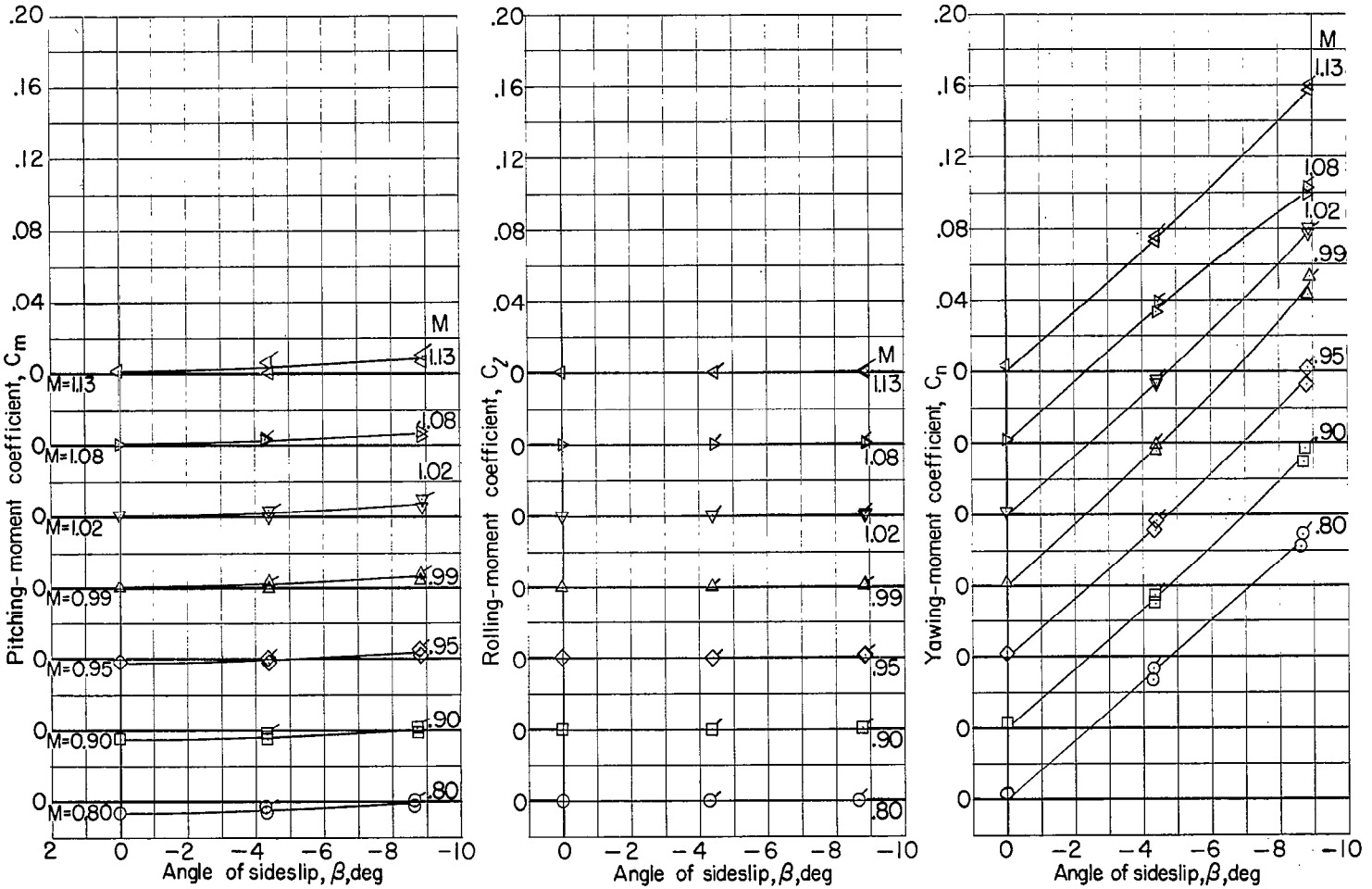

(a) $\alpha = 0^\circ$.

Figure 7.- Aerodynamic coefficients for canopy 2. (Flagged symbols indicate data at positive sideslip angles.)

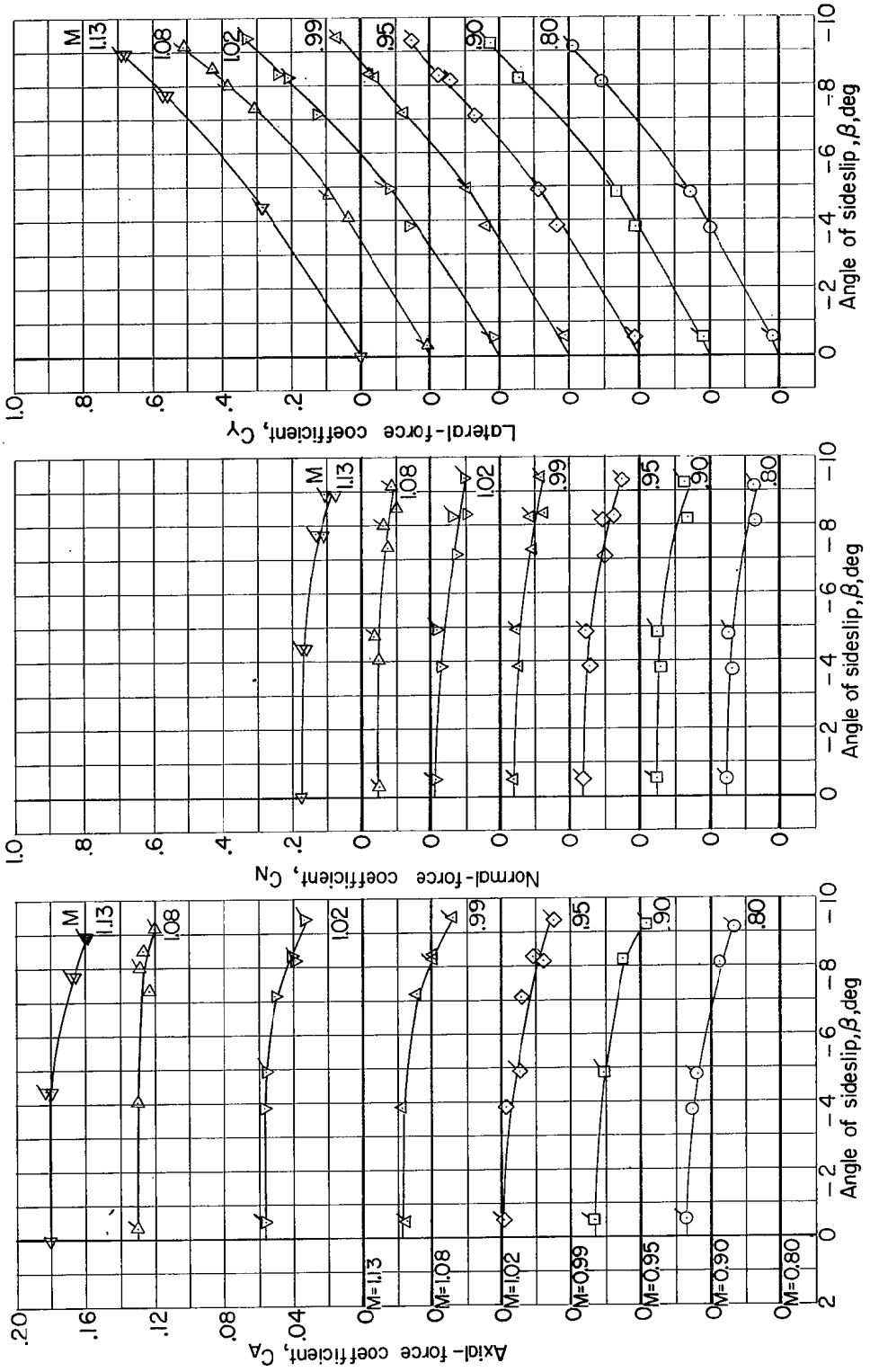
Axial-force coefficient, C_A
Normal-force coefficient, C_N
Lateral-force coefficient, C_Y
Angle of sideslip, β, deg
M
1.13
1.08
1.02
.99
.95
.90
.80
$M=1.13$
$M=1.08$
$M=1.02$
$M=0.99$
$M=0.95$
$M=0.90$
$M=0.80$

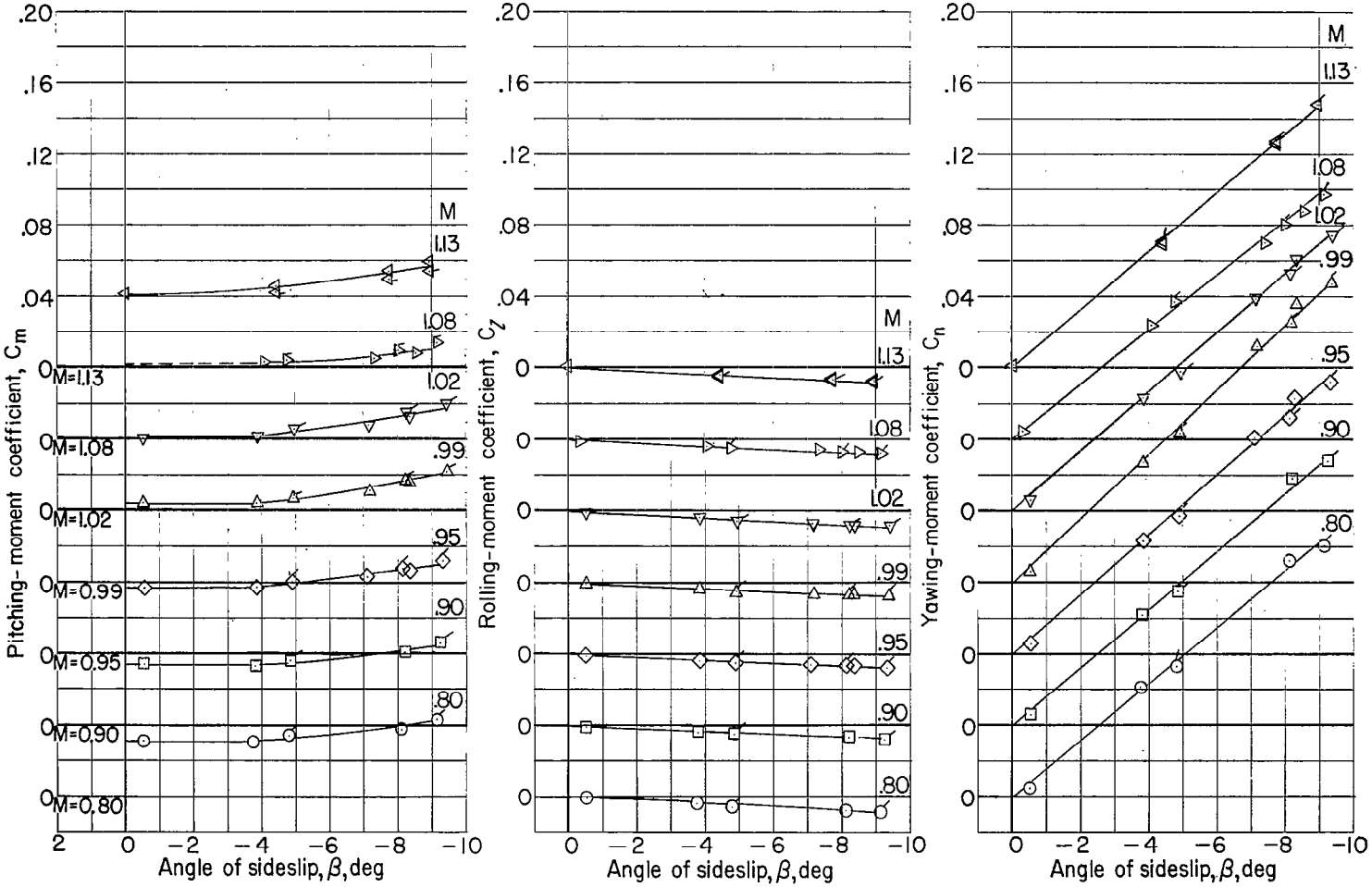

(b) $\alpha = 5.1^{\circ}$.

Figure 7.- Continued.

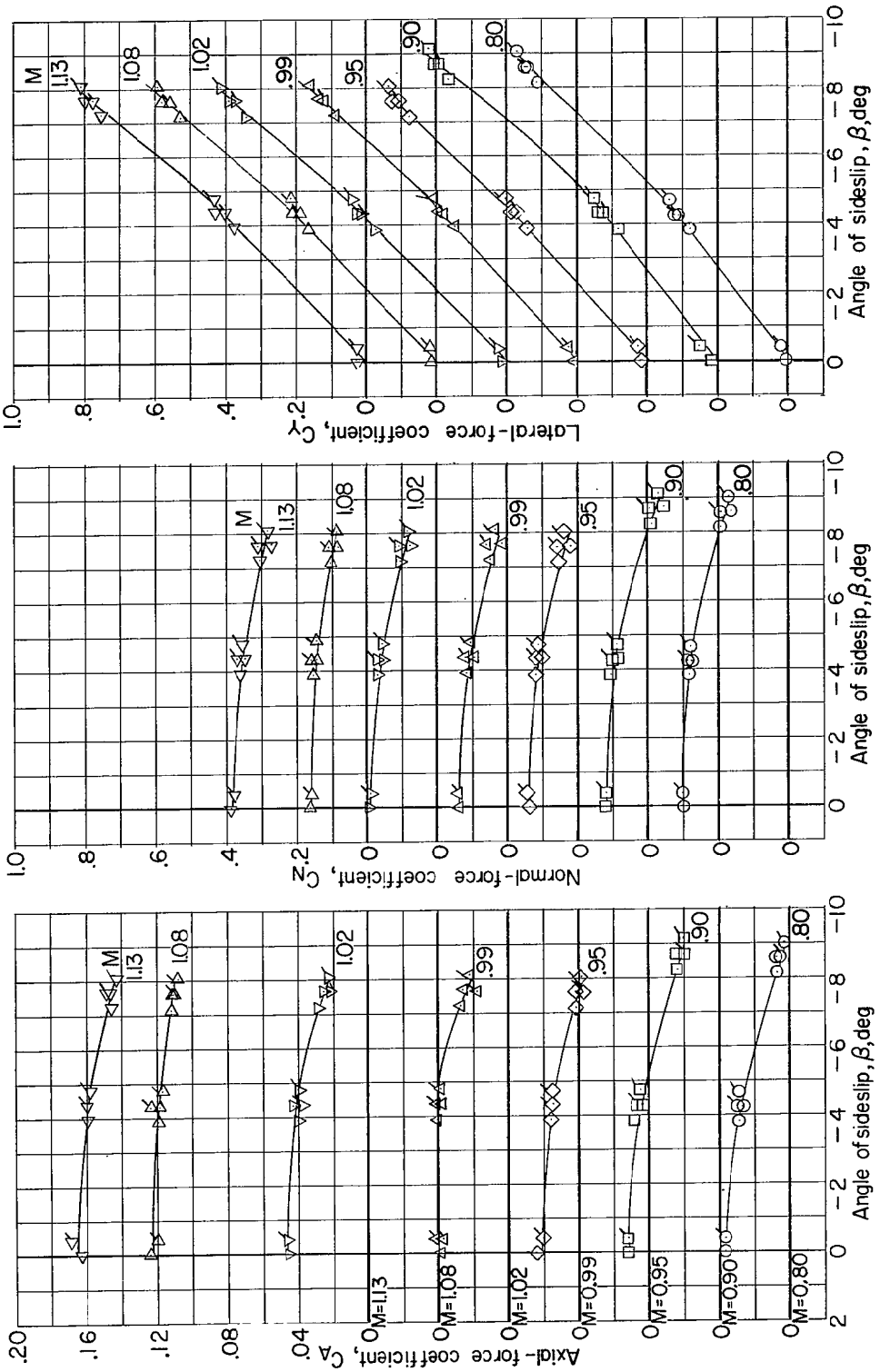
Axial-force coefficient, C_A
Normal-force coefficient, C_N
Lateral-force coefficient, C_Y
Angle of sideslip, β, deg
M
1.13
1.08
1.02
.99
.95
.90
.80
M=1.13
M=1.08
M=1.02
M=0.99
M=0.95
M=0.90
M=0.80

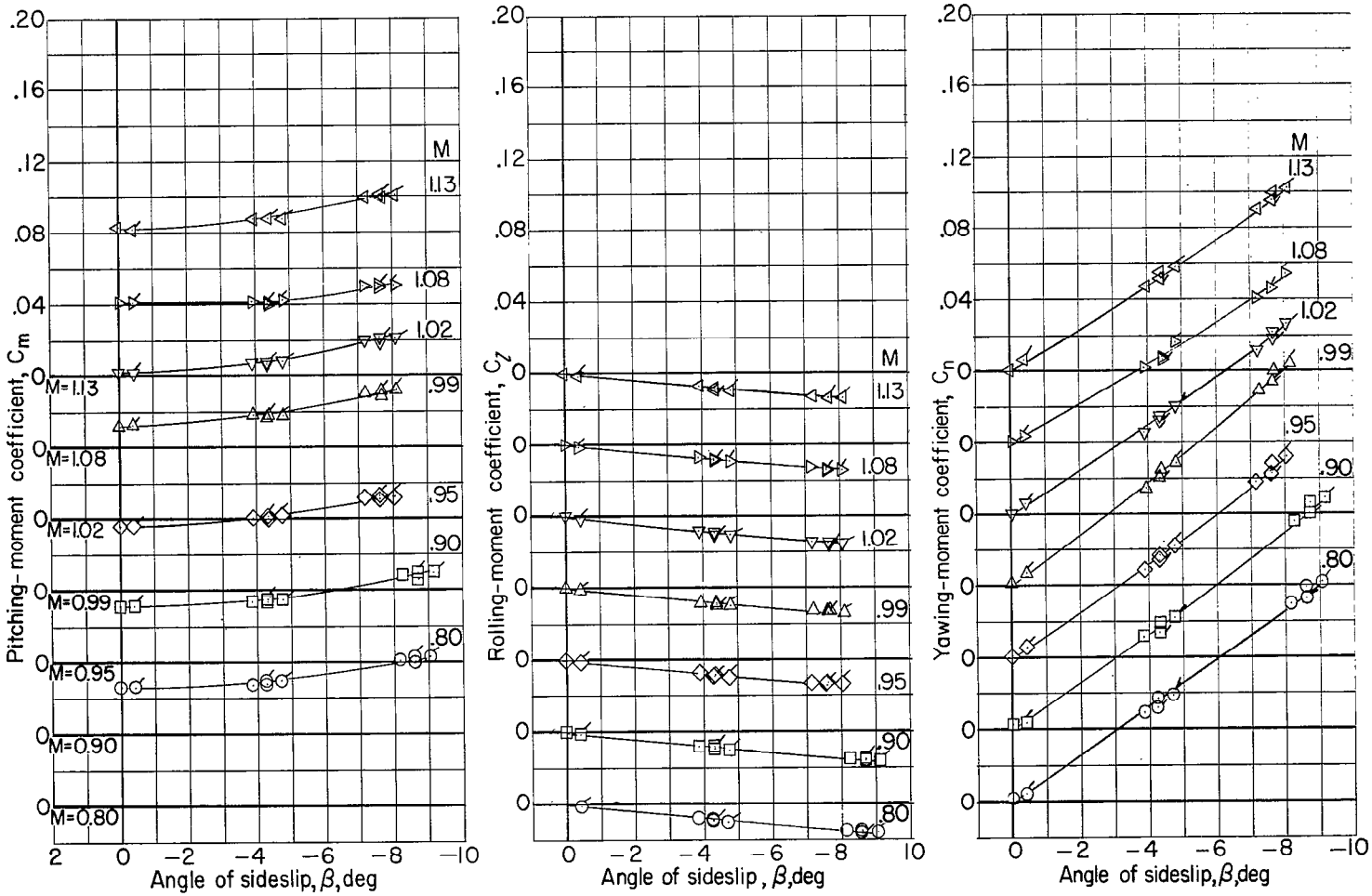

(c) $\alpha = 10.3^{\circ}$.

Figure 7.- Concluded.

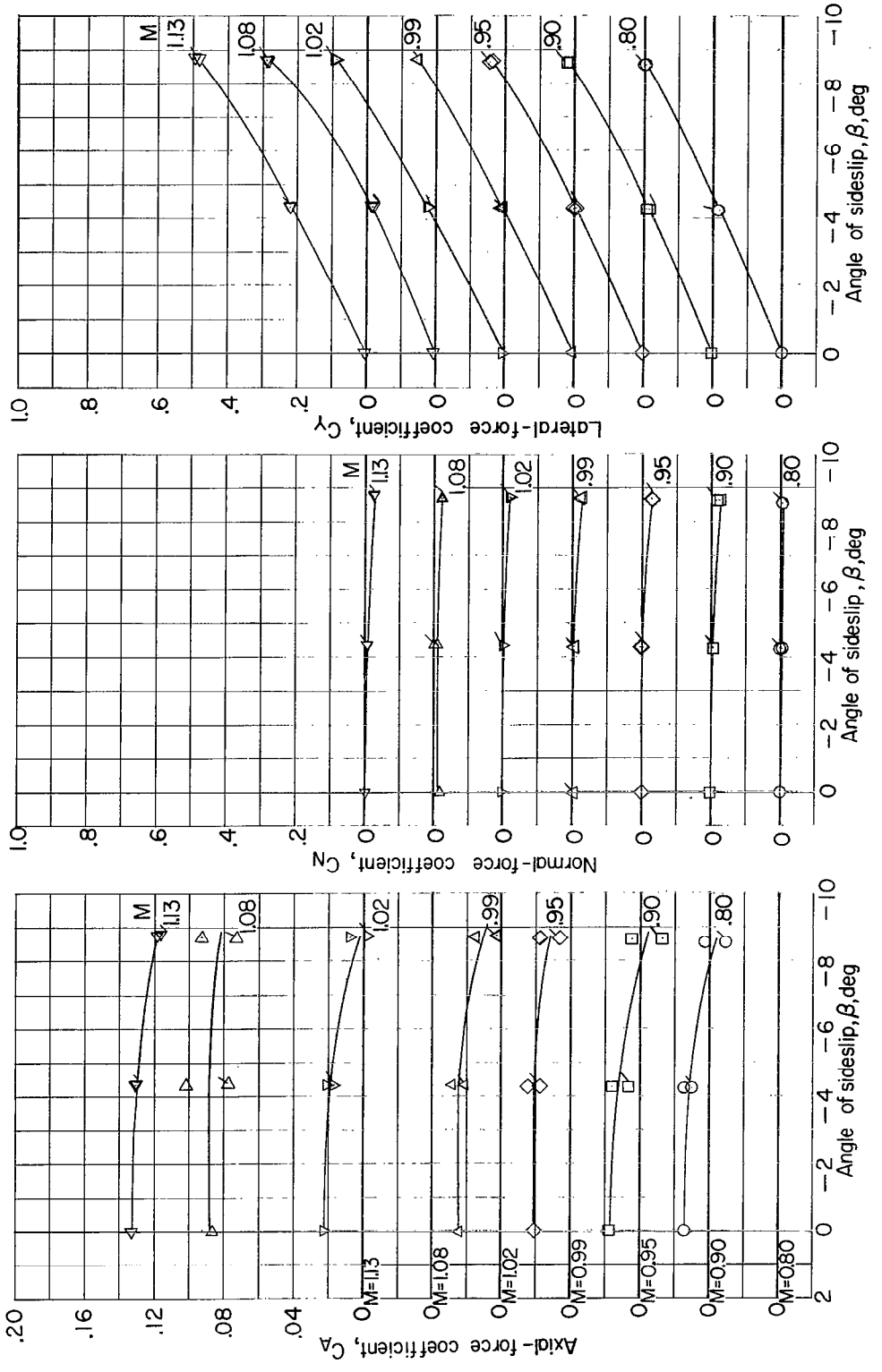
Axial-force coefficient, C_A
Normal-force coefficient, C_N
Lateral-force coefficient, C_Y
Angle of sideslip, β, deg
M
1.13
1.08
1.02
.99
.95
.90
.80
$M_{M=1.13}$
$M_{M=1.08}$
$M_{M=1.02}$
$M_{M=0.99}$
$M_{M=0.95}$
$M_{M=0.90}$
$M_{M=0.80}$

[redacted]

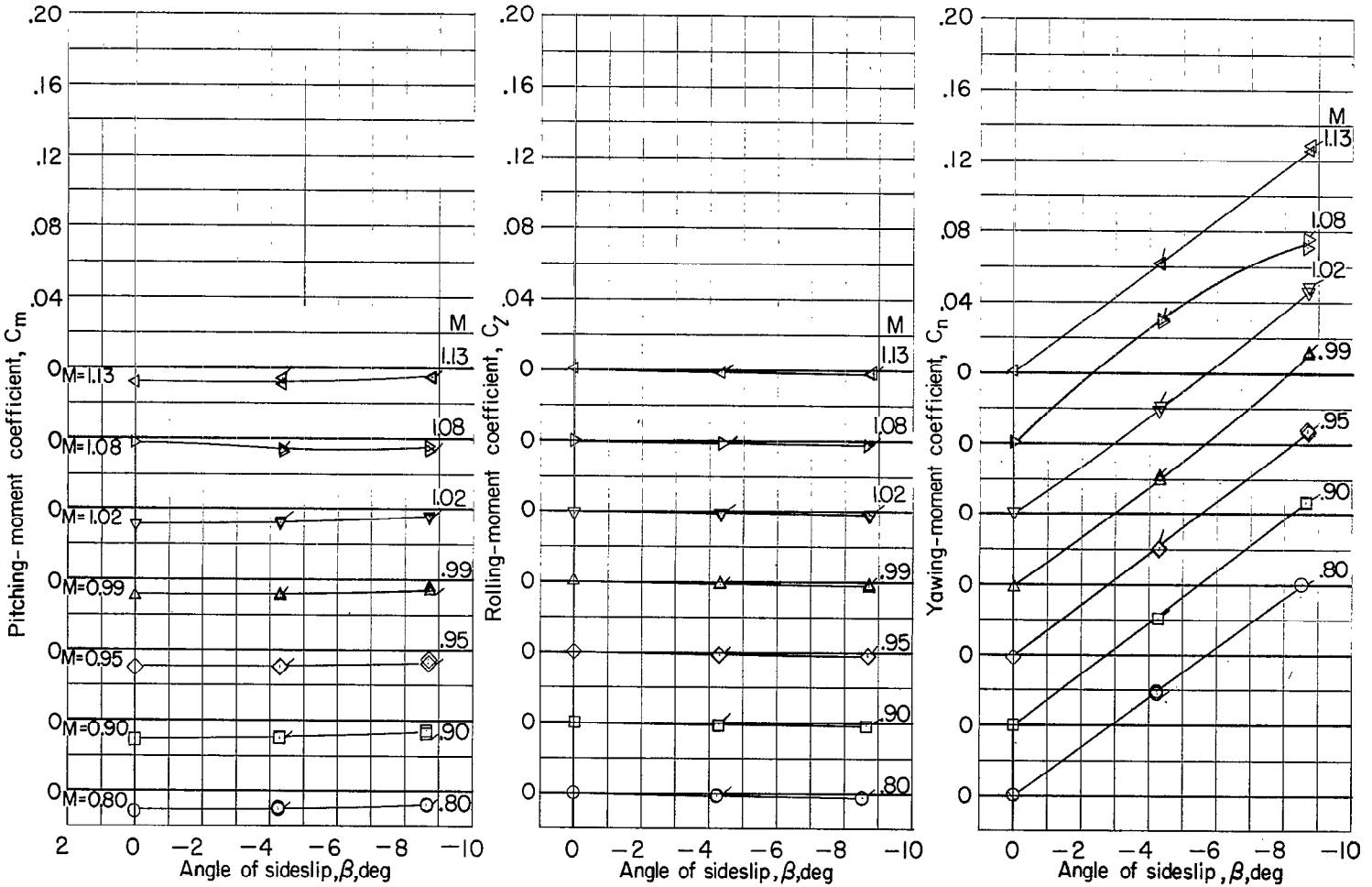

(a) $\alpha = 0^\circ$.

Figure 8.- Aerodynamic coefficients for canopy 3. (Flagged symbols indicate data at positive sldeslip angles.)

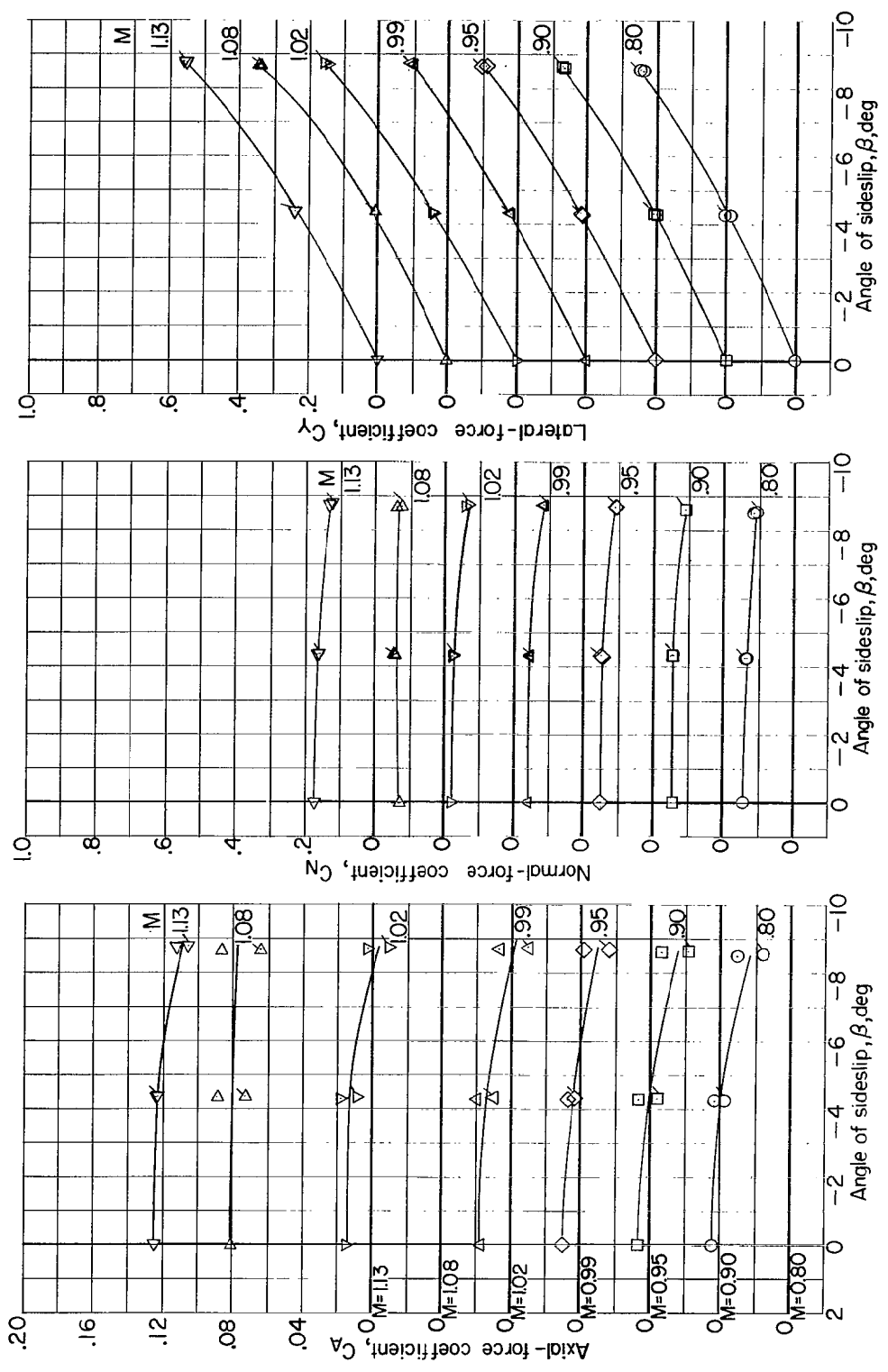
Axial-force coefficient, C_A
Normal-force coefficient, C_N
Lateral-force coefficient, C_Y
Angle of sideslip, β, deg
M
1.13
1.08
1.02
.99
.95
.90
.80
M=1.13
M=1.08
M=1.02
M=0.99
M=0.95
M=0.90
M=0.80

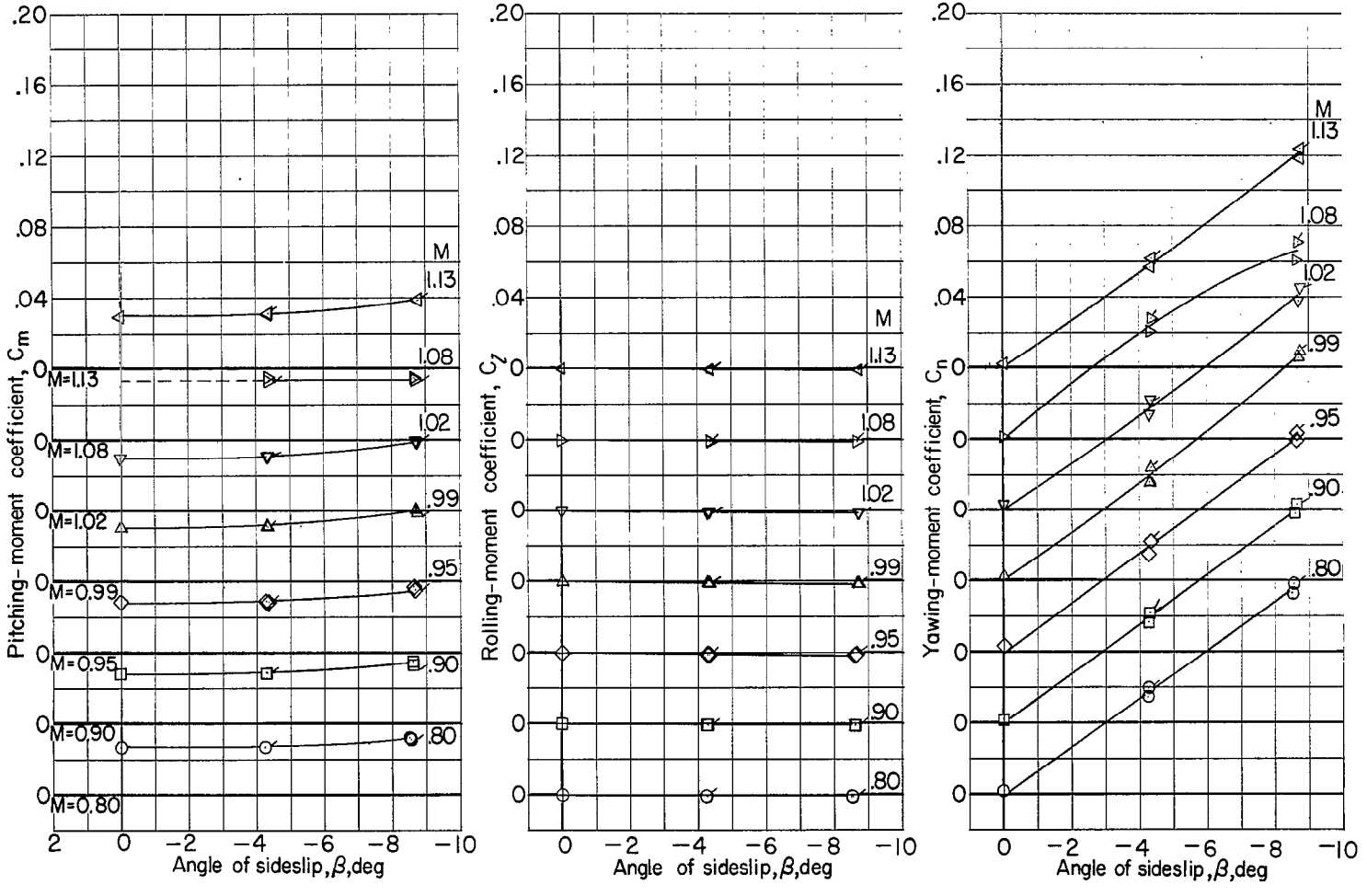

(b) $\alpha = 5.1^\circ$.

Figure 8.- Continued.

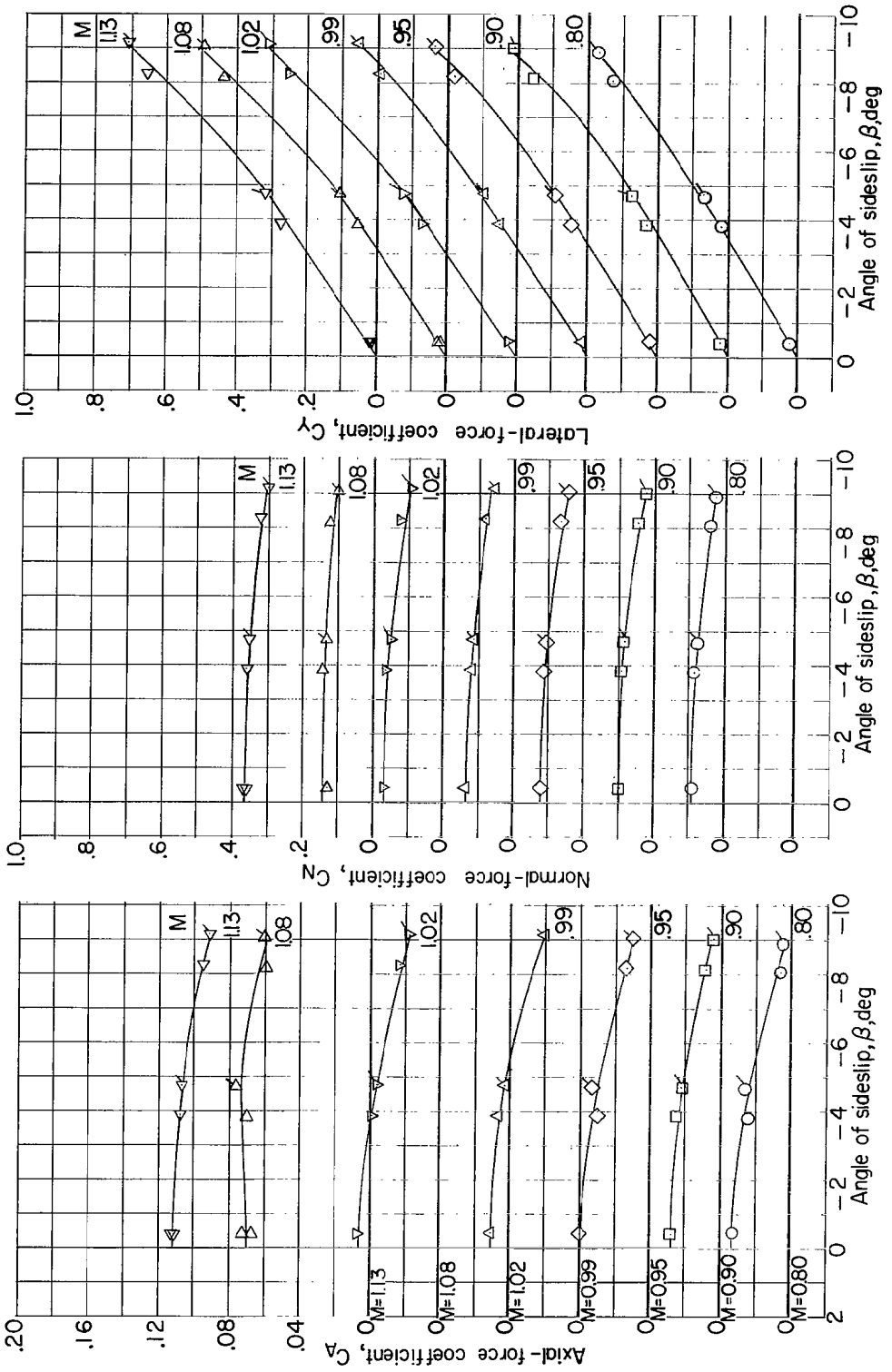
Axial-force coefficient, C_A
Normal-force coefficient, C_N
Lateral-force coefficient, C_Y
Angle of sideslip, β, deg
M
1.13
1.08
1.02
.99
.95
.90
.80
$M=1.13$
$M=1.08$
$M=1.02$
$M=0.99$
$M=0.95$
$M=0.90$
$M=0.80$

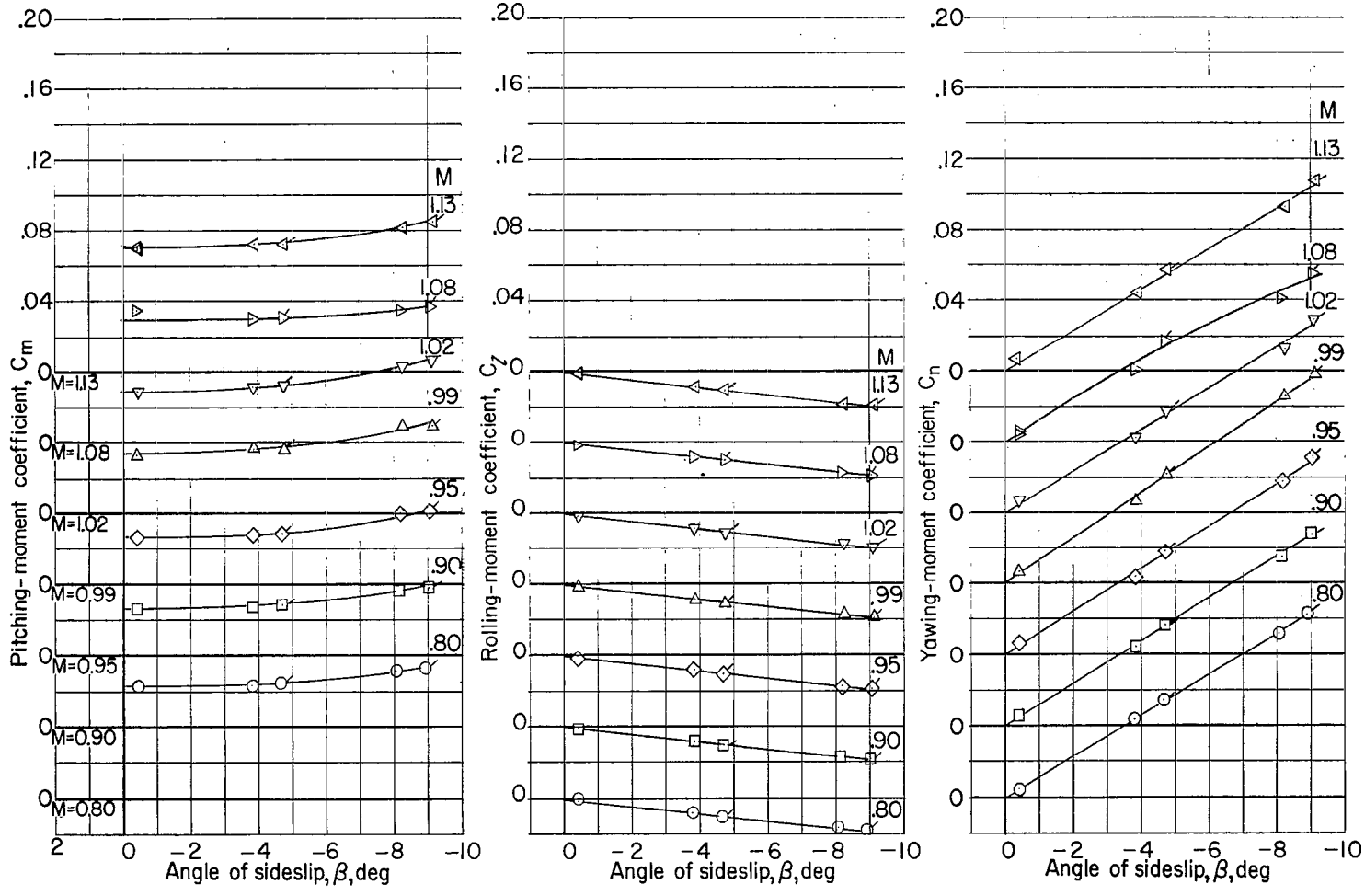

(c) $\alpha = 10.3^{\circ}$.

Figure 8.- Concluded.

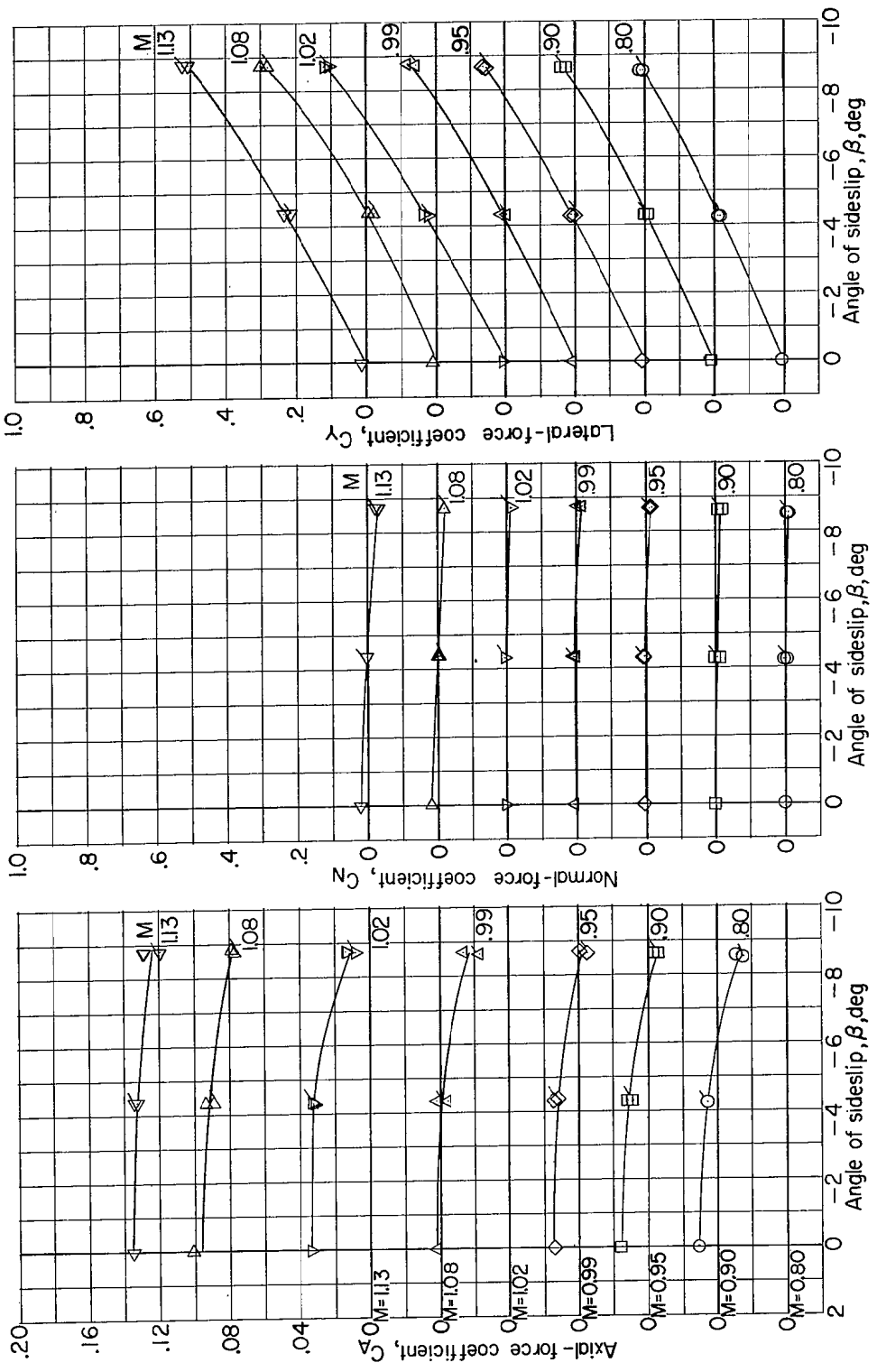
Axial-force coefficient, C_A
Normal-force coefficient, C_N
Lateral-force coefficient, C_Y
Angle of sideslip, β, deg
M
1.13
1.08
1.02
.99
.95
.90
.80
$M=1.13$
$M=1.08$
$M=1.02$
$M=0.99$
$M=0.95$
$M=0.90$
$M=0.80$

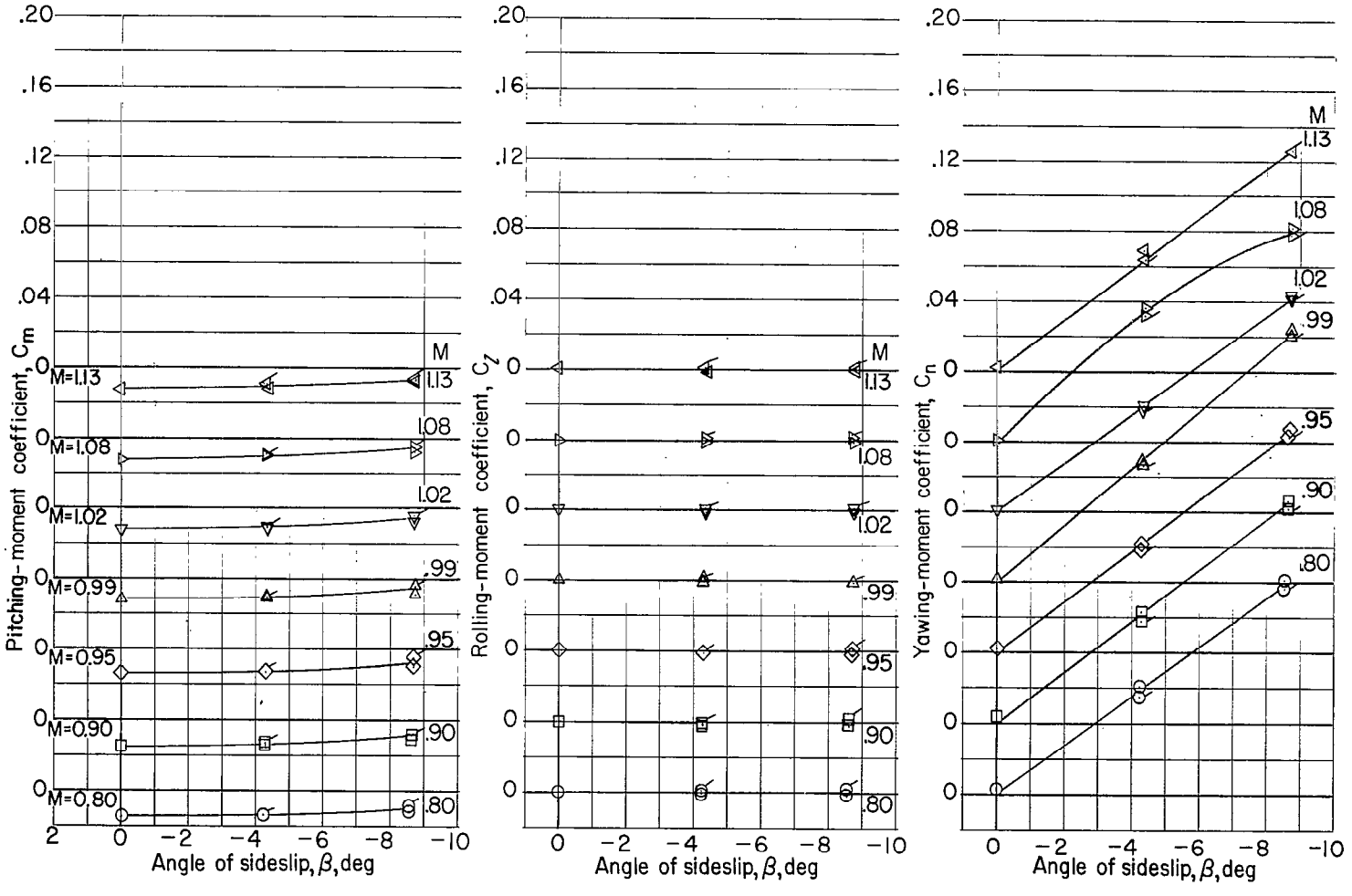

(a) $\alpha = 0^\circ$.

Figure 9.- Aerodynamic coefficients for canopy 4. (Flagged symbols indicate data at positive sideslip angles.)

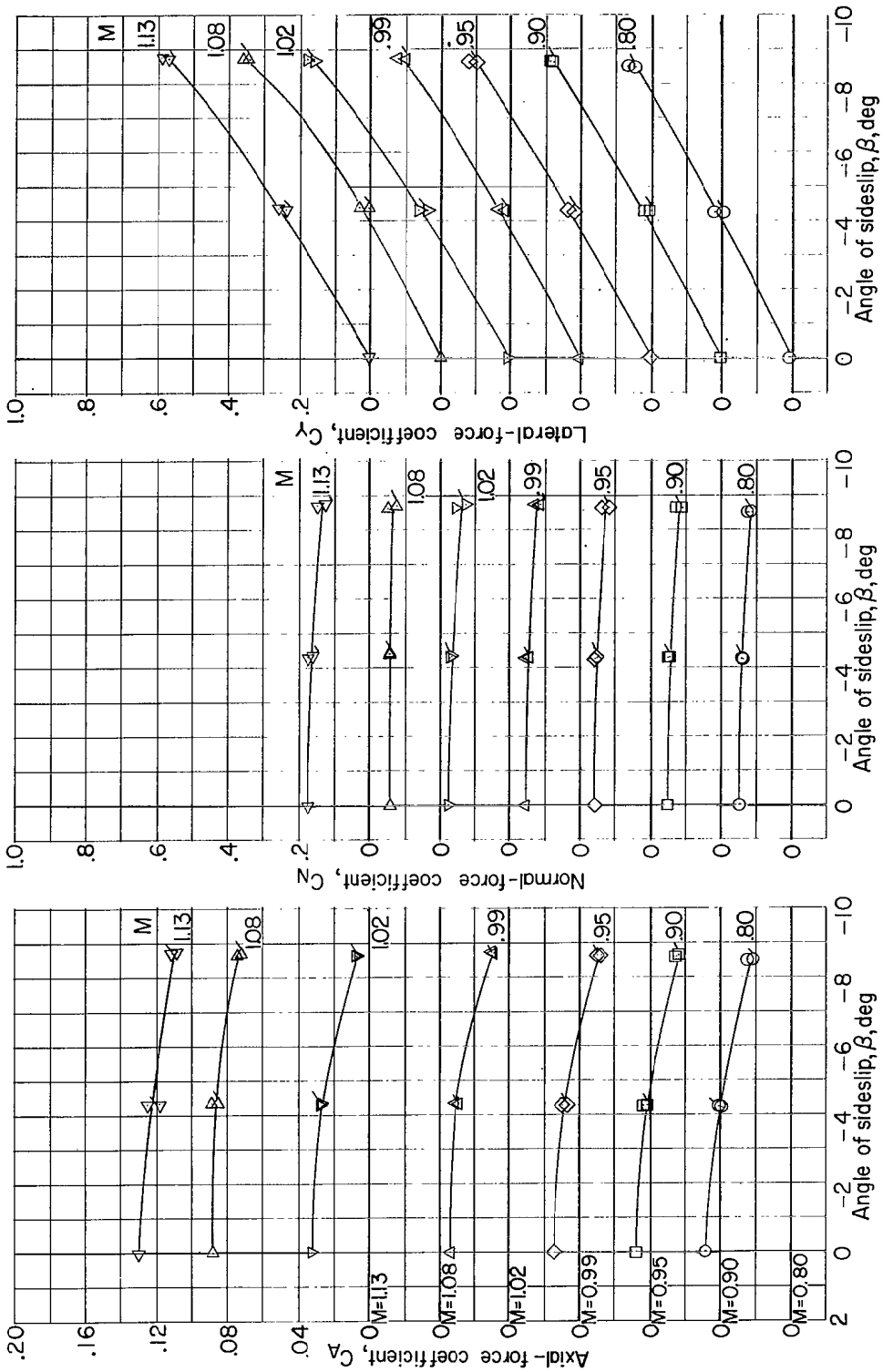
Axial-force coefficient, C_A
Normal-force coefficient, C_N
Lateral-force coefficient, C_Y
Angle of sideslip, β, deg
M
1.13
1.08
1.02
.99
.95
.90
.80
$M=1.13$
$M=1.08$
$M=1.02$
$M=0.99$
$M=0.95$
$M=0.90$
$M=0.80$

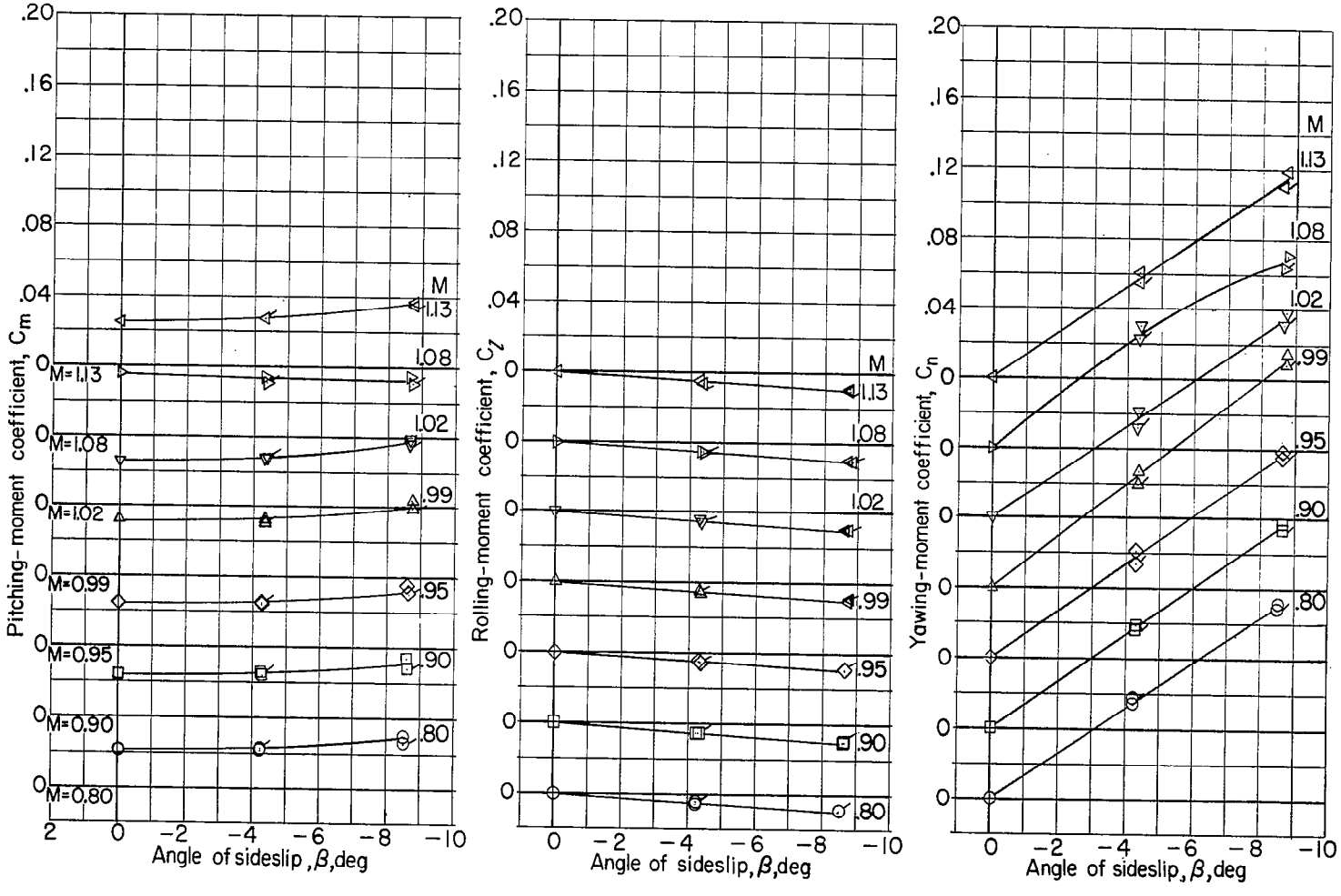

(b) $\alpha = 5.1^\circ$.

Figure 9.- Continued.

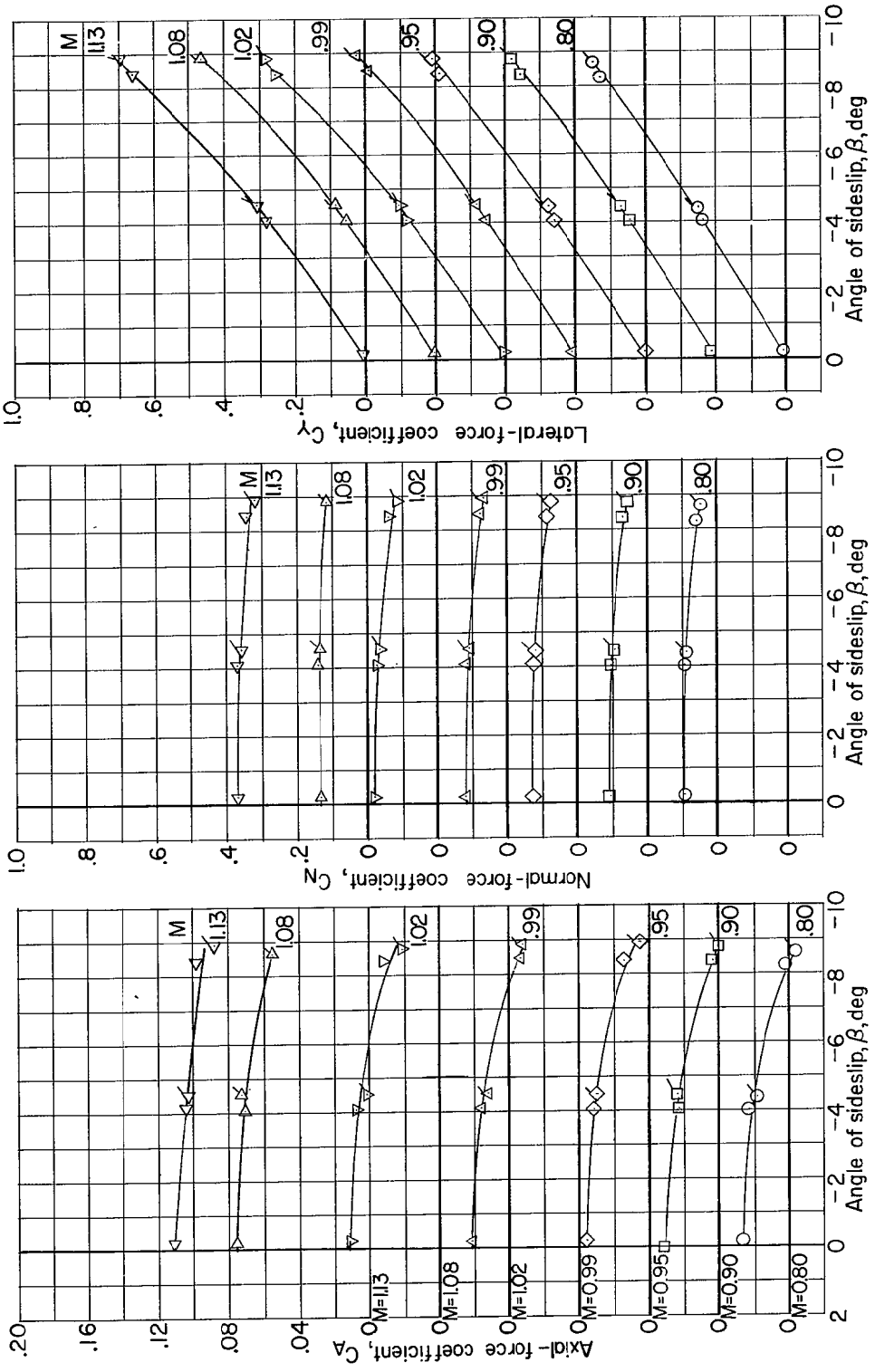
Axial-force coefficient, C_A
Normal-force coefficient, C_N
Lateral-force coefficient, C_Y
Angle of sideslip, β, deg
M
1.13
1.08
1.02
.99
.95
.90
.80
M=1.13
M=1.08
M=1.02
M=0.99
M=0.95
M=0.90
M=0.80

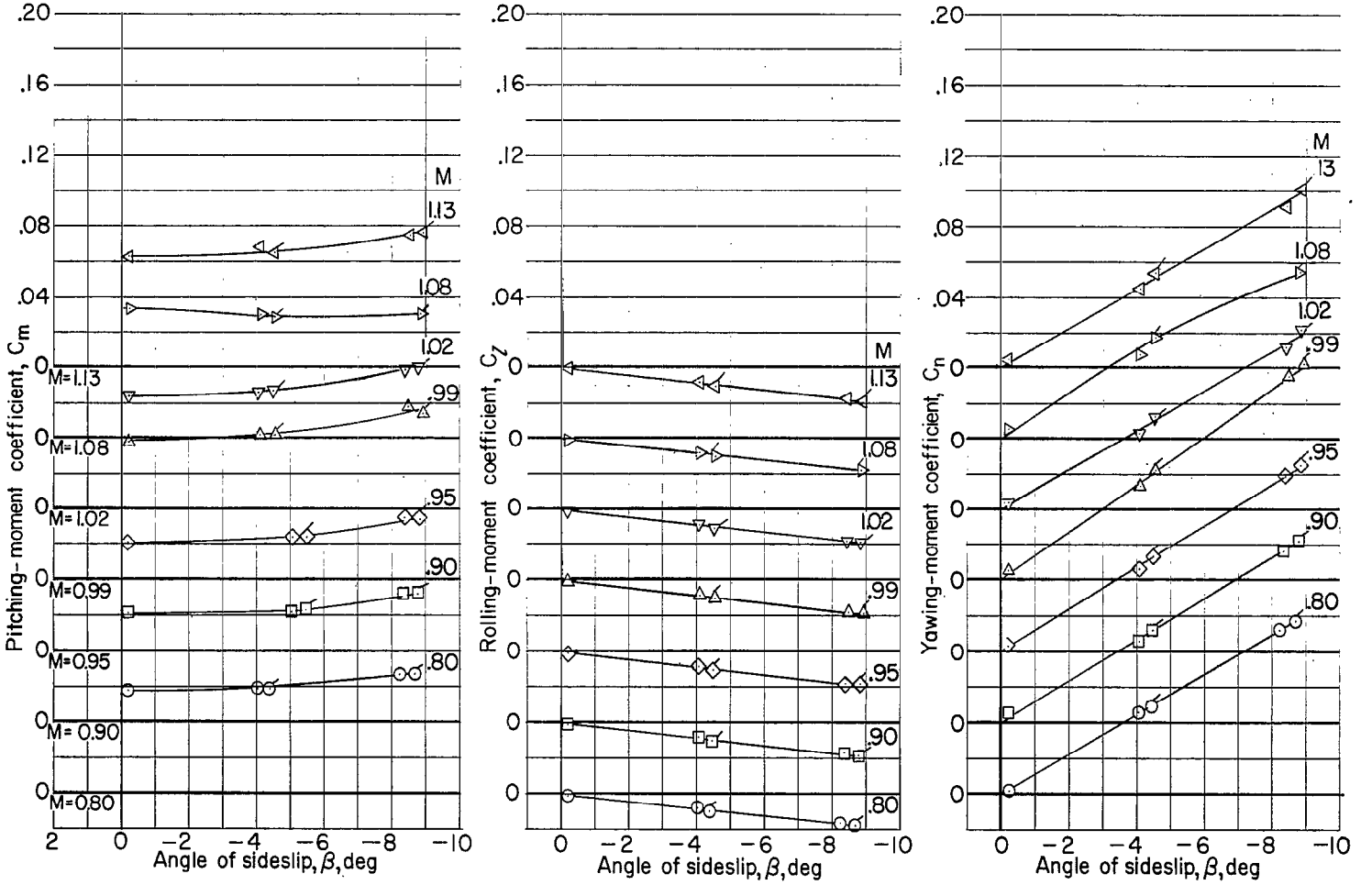

(c) $\alpha = 10.2^{\circ}$.

Figure 9.- Concluded.

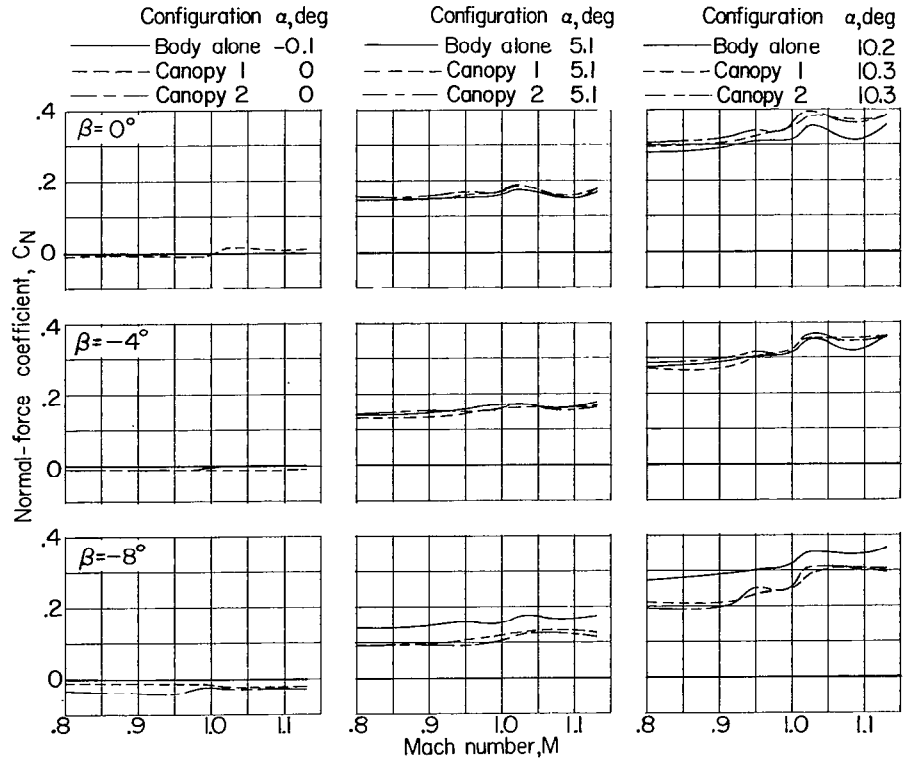

(a) Normal-force coefficient.

Figure 10.- Effect of windshield shape.

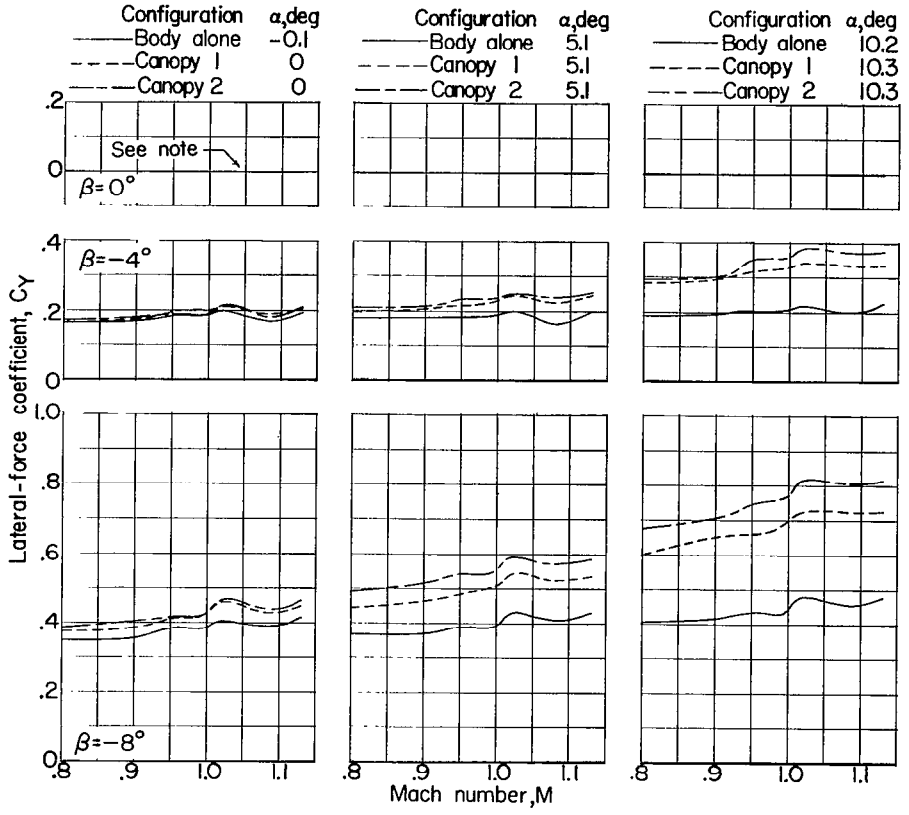

(b) Lateral-force coefficient. Note: All C_y values are zero for $\beta = 0^\circ$.

Figure 10.- Continued.

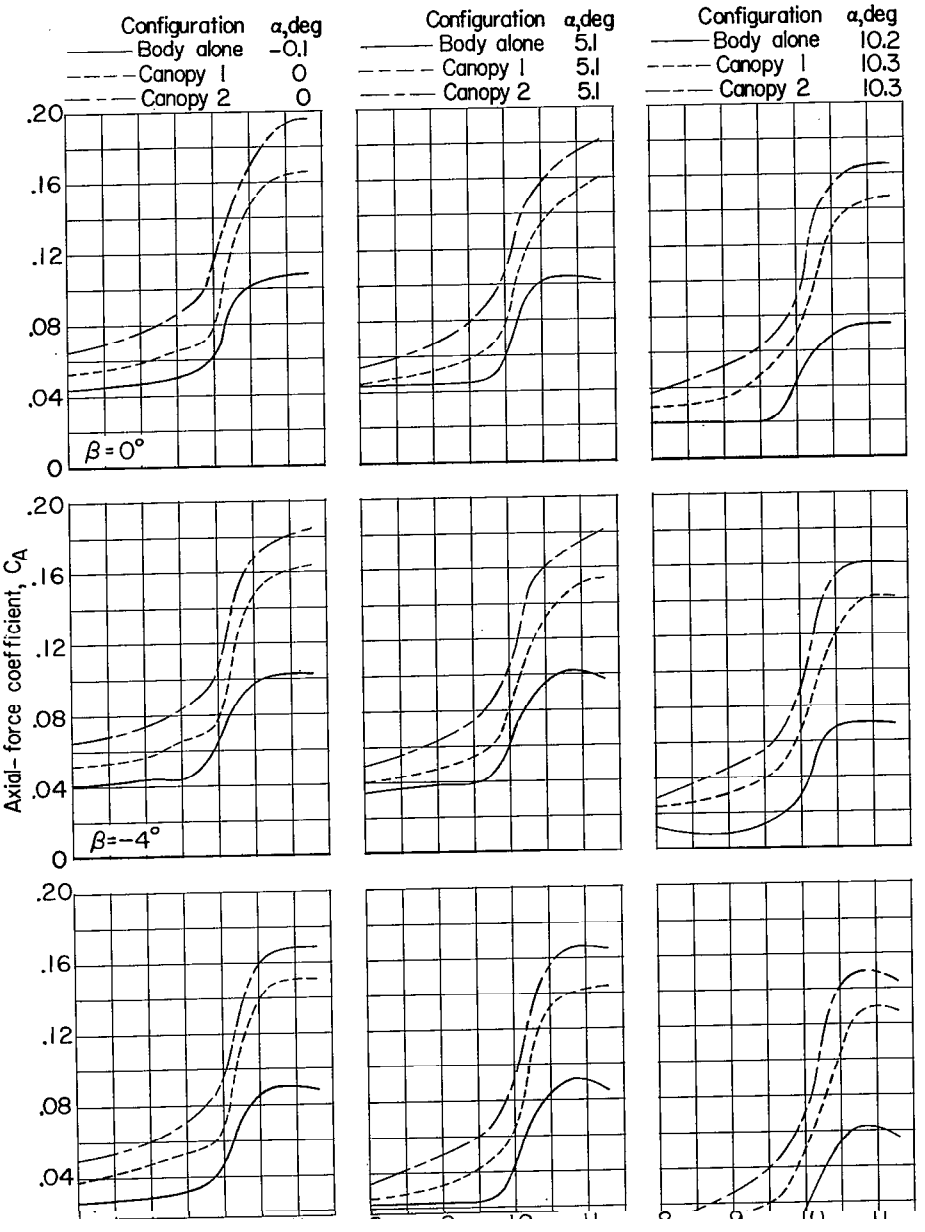
Configuration
Body alone
Canopy 1
Canopy 2
α,deg
−0.1
0
0
5.1
5.1
5.1
10.2
10.3
10.3
Axial-force coefficient, C_A
.20
.16
.12
.08
.04
0
β = 0°
β = −4°

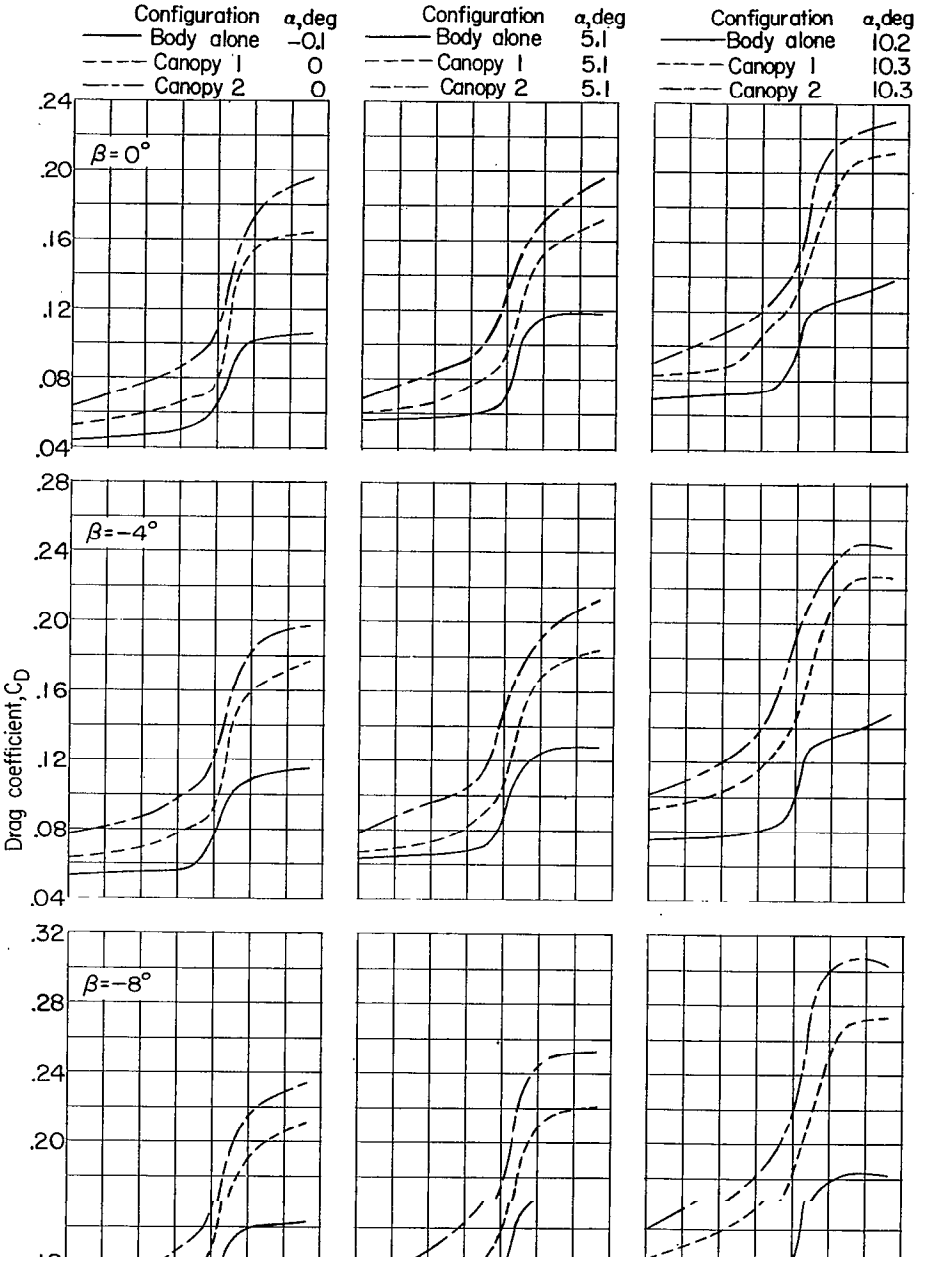
Configuration
Body alone
Canopy 1
Canopy 2
α, deg
−0.1
0
0
Configuration
Body alone
Canopy 1
Canopy 2
α, deg
5.1
5.1
5.1
Configuration
Body alone
Canopy 1
Canopy 2
α, deg
10.2
10.3
10.3
β = 0°
β = −4°
β = −8°
Drag coefficient, C_D
.24
.20
.16
.12
.08
.04
.28
.24
.20
.16
.12
.08
.04
.32
.28
.24
.20

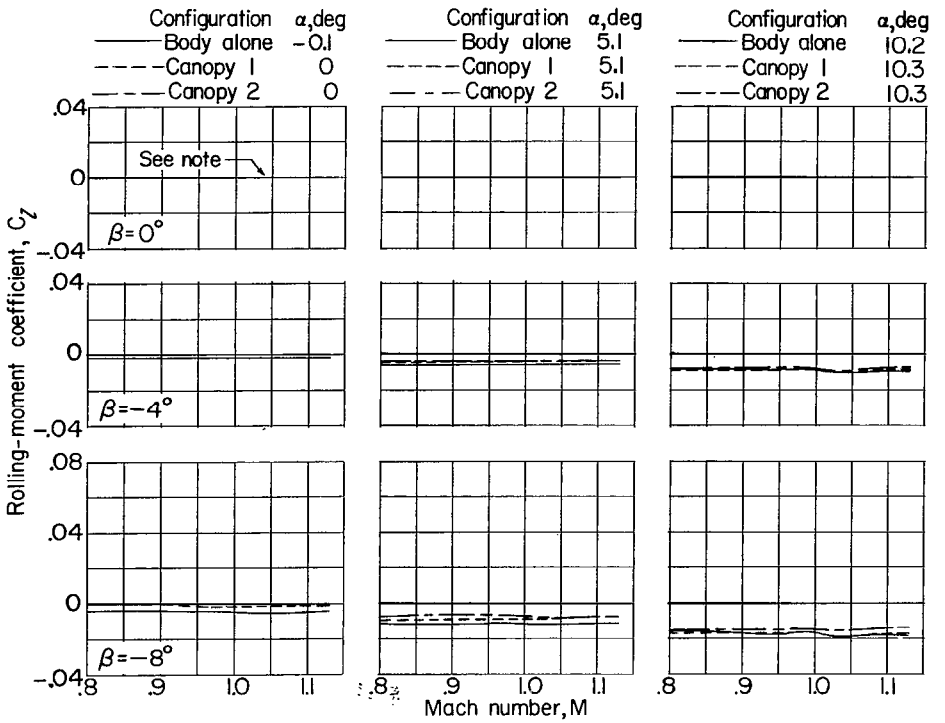

(e) Rolling-moment coefficient. Note: All C_l values are zero for $\beta = 0^\circ$.

Figure 10.- Continued.

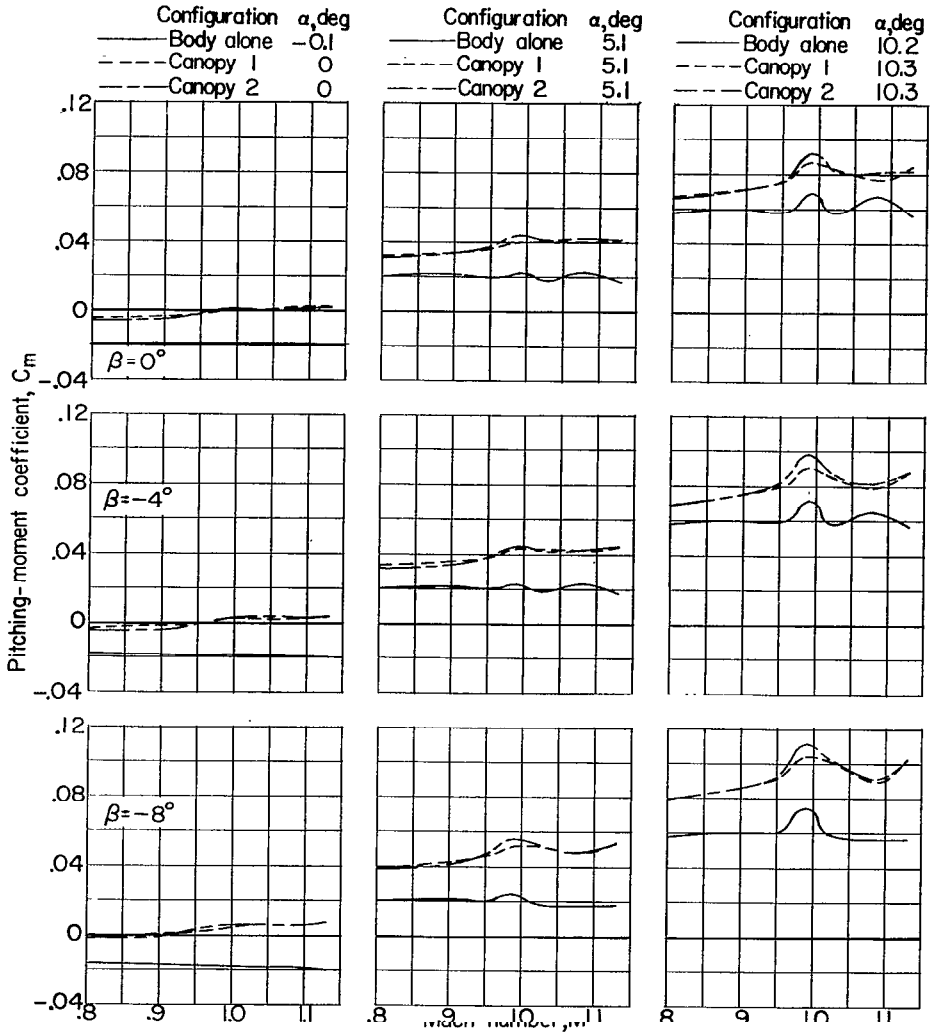
Configuration α,deg
Body alone −0.1
Canopy 1 0
Canopy 2 0
Configuration α,deg
Body alone 5.1
Canopy 1 5.1
Canopy 2 5.1
Configuration α,deg
Body alone 10.2
Canopy 1 10.3
Canopy 2 10.3
Pitching-moment coefficient, Cm
.12
.08
.04
0
-.04
β=0°
β=-4°
β=-8°
.8
.9
1.0
1.1

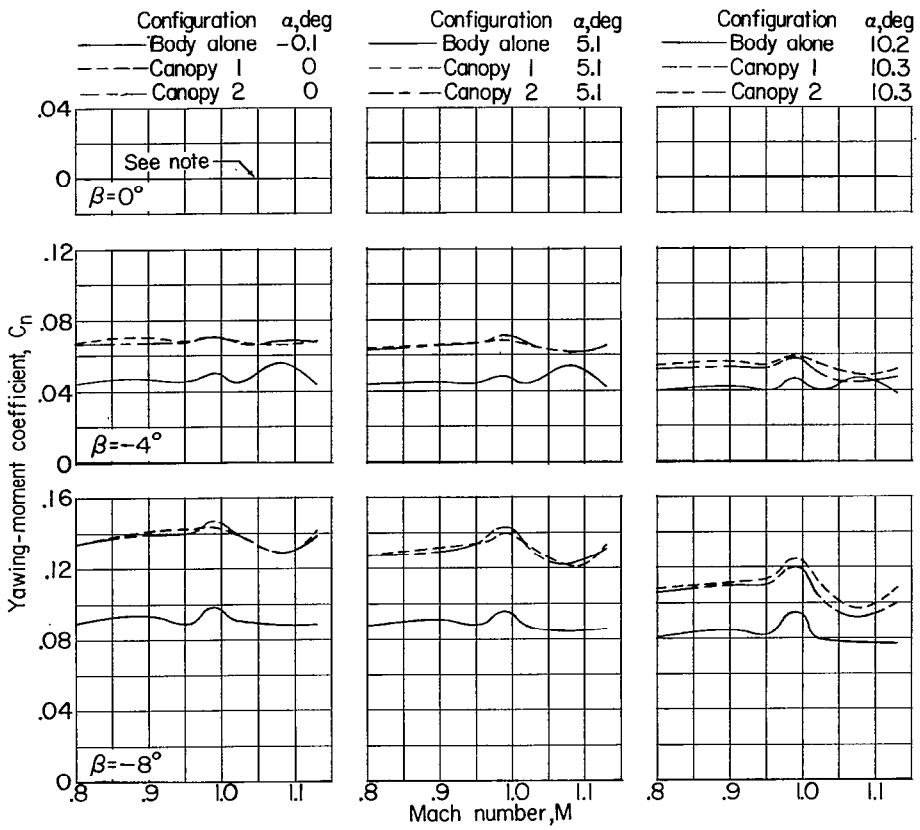

(g) Yawing-moment coefficient. Note: All C_n values are zero for $\beta = 0^\circ$.

Figure 10.- Concluded.

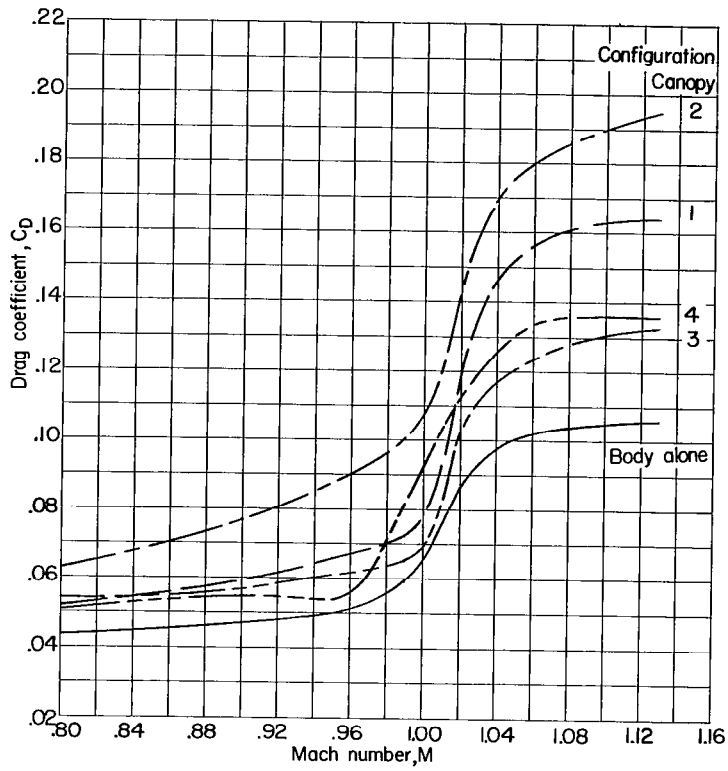

Figure 11.- Comparison of drag for the five models tested. $\beta = 0^{\circ}$; $\alpha = 0^{\circ}$ (approx.).